An Integrated Global Analysis of Compartmentalized HRAS Signaling

Resource

Cell Reports

An Integrated Global Analysis of Compartmentalized HRAS Signaling

Graphical Abstract

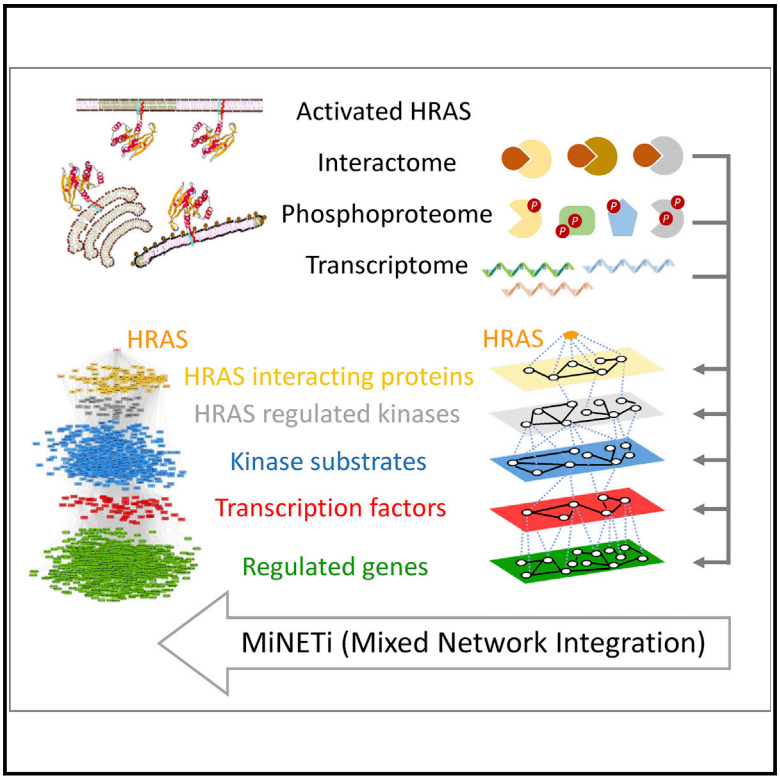

Authors

Tapesh Santra, Ana Herrero, Javier Rodriguez, ..., Piero Crespo, David Matallanas, Walter Kolch

Correspondence

david.gomez@ucd.ie (D.M.), walter.kolch@ucd.ie (W.K.)

In Brief

Santra et al. develop MiNETi (Mixed Network Integration) to integrate multi-omics data. Applying MiNETi to analyze the interactome, phosphoproteome, and transcriptome regulated by HRAS signaling from different subcellular compartments shows that HRAS controls phosphorylation-dependent signaling mainly from the cell membrane but regulates a large number of genes from endomembranes.

Highlights

- MiNETi (Mixed Network Integration) enables the integration of multi-omics datasets
- MiNETi provides an integrated view of HRAS signaling from different subcellular sites
- HRAS controls its interactome, phosphoproteome, and transcriptome site specifically
- HRAS regulates cell migration and p53-mediated apoptosis from endomembranes

Santra et al., 2019, Cell Reports *26*, 3100–3115
March 12, 2019
https://doi.org/10.1016/j.celrep.2019.02.038

CellPress

OPEN ACCESS
CellPress

Cell Reports
Resource

An Integrated Global Analysis of Compartmentalized HRAS Signaling

Tapesh Santra,[1,7] Ana Herrero,[1,7,8] Javier Rodriguez,[1,8] Alex von Kriegsheim,[1,8] Luis F. Iglesias-Martinez,[1] Thomas Schwarzl,[1,9] Des Higgins,[1,2,3] Thin-Thin Aye,[4] Albert J.R. Heck,[4] Fernando Calvo,[5] Lorena Agudo-Ibáñez,[5] Piero Crespo,[5,6] David Matallanas,[1,10,*] and Walter Kolch[1,2,3,*]

[1]Systems Biology Ireland, University College Dublin, Belfield, Dublin, Ireland
[2]Conway Institute of Biomolecular & Biomedical Research, University College Dublin, Belfield, Ireland
[3]School of Medicine and Medical Science, University College Dublin, Belfield, Ireland
[4]Biomolecular Mass Spectrometry and Proteomics, Bijvoet Centre for Biomolecular Research and Utrecht Institute for Pharmaceutical Science, Utrecht University, Padualaan 8, 3584 Utrecht, the Netherlands
[5]Instituto de Biomedicina y Biotecnología de Cantabria (IBBTEC), Consejo Superior de Investigaciones Científicas (CSIC) - Universidad de Cantabria, Santander 39011, Spain
[6]Centro de Investigación Biomédica en Red de Cáncer (CIBERONC), Instituto de Salud Carlos III, Madrid, Spain
[7]These authors contributed equally
[8]Present address: Edinburgh Cancer Research UK Centre, Institute of Genetics and Molecular Medicine, University of Edinburgh, Edinburgh, UK
[9]Present address: Genome Biology Unit, European Molecular Biology Laboratory, 69117 Heidelberg, Germany
[10]Lead Contact
*Correspondence: david.gomez@ucd.ie (D.M.), walter.kolch@ucd.ie (W.K.)
https://doi.org/10.1016/j.celrep.2019.02.038

SUMMARY

Modern omics technologies allow us to obtain global information on different types of biological networks. However, integrating these different types of analyses into a coherent framework for a comprehensive biological interpretation remains challenging. Here, we present a conceptual framework that integrates protein interaction, phosphoproteomics, and transcriptomics data. Applying this method to analyze HRAS signaling from different subcellular compartments shows that spatially defined networks contribute specific functions to HRAS signaling. Changes in HRAS protein interactions at different sites lead to different kinase activation patterns that differentially regulate gene transcription. HRAS-mediated signaling is the strongest from the cell membrane, but it regulates the largest number of genes from the endoplasmic reticulum. The integrated networks provide a topologically and functionally resolved view of HRAS signaling. They reveal distinct HRAS functions including the control of cell migration from the endoplasmic reticulum and TP53-dependent cell survival when signaling from the Golgi apparatus.

INTRODUCTION

While extensive analysis methods exist for individual types of omics data, integrating data into a connected view or single network is a grand challenge in biology that has attracted many approaches to solve it (Huang et al., 2017). Most efforts have focused on integrating features on a binary level, such as relationships between mRNA and protein expression (Haider and Pal, 2013) and the correlation between global molecular data and disease phenotypes (Gibbs et al., 2014; Imielinski et al., 2012; Stingele et al., 2012; Wu et al., 2014; Zhang et al., 2014). The global integration of omics data is impeded by the different types of data, their heterogeneity, different levels of completeness, indeterminate mapping to each other, and uncertain temporal relationships between them. Efforts to overcome these limitations largely have used methods for dimensionality reduction and correlative detection of regularities, i.e., features common to different data types (Huang et al., 2017; Rohart et al., 2017). However, these methods do not take into account mechanistic relationships, which is desirable for modeling that is predictive and can consider chains of biochemical and biological events.

In response to these requirements, we have developed a conceptual framework, MiNETi (Mixed Network Integration) that reconstructs and integrates interaction proteomics, phosphoproteomics, and transcriptomics data in an organic way. MiNETi considers statistical and mechanistic relationships and operates in four stages. First, it analyzes protein interactome, phosphoproteomics, and transcriptomic data to reconstruct protein-protein interaction (PPI), kinase-substrate (KS), and transcription factor (TF)-DNA interaction networks. These networks are then linked using prior knowledge from PPI databases to construct integrated networks that can be used to track signals emanating from multiprotein complexes and are transmitted via phosphorylation networks to the nucleus, where they modify the activities of transcriptional regulators to control changes in gene expression. MiNETi is universally applicable to datasets where PPI changes regulate gene transcription via phosphorylation networks.

Here, we have used MiNETi to analyze compartmentalized HRAS signaling. HRAS belongs to the RAS family of GTPases,

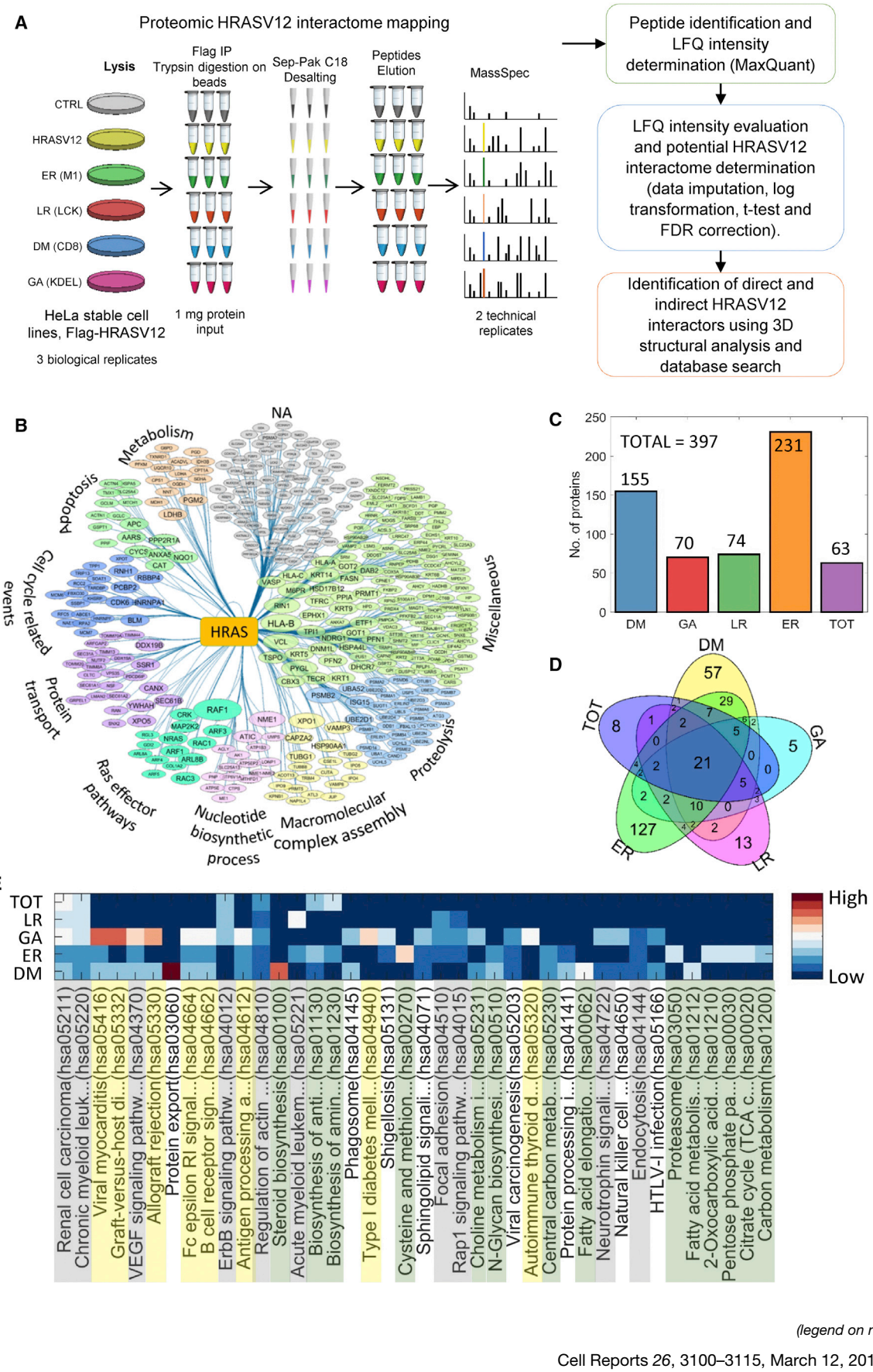

(legend on next page)

which play key roles in human cancer. Activating RAS mutations are found in 20%–30% of human cancers, especially in common cancers such as colorectal, lung, and pancreatic cancer (Cox et al., 2014; Karnoub and Weinberg, 2008). RAS mutations are typically associated with poor prognosis and therapy resistance (Cox et al., 2014). In the absence of clinically successful RAS inhibitors, efforts have focused on targeting downstream effector pathways. However, these approaches are hampered by the large number of RAS effector pathways and the intricacies of the functional interactions between them (Pylayeva-Gupta et al., 2011). For instance, inhibition of AKT and ERK, two main effector pathways, can be synergistic or antagonistic (Liu et al., 2012). Thus, an exact and comprehensive understanding of the downstream signaling networks regulated by activated RAS is essential for designing efficacious interventions. An added complication is that RAS can signal from different subcellular compartments (Chiu et al., 2002; Daniels et al., 2006; Matallanas et al., 2006; Rocks et al., 2005). This spatial aspect of RAS signaling can modulate activation kinetics (Lorentzen et al., 2010), rewiring of pathways by controlling scaffolding protein interactions (Casar et al., 2009), and biological responses such as proliferation, apoptosis, and differentiation (Aran and Prior, 2013; Chiu et al., 2002; Daniels et al., 2006).

These studies focusing on selected pathways have highlighted the importance of compartmentalized RAS signaling, but a systematic global analysis is lacking. Therefore, we applied MiNETi to reconstruct and analyze global signaling networks regulated by activated HRAS from the disordered cell membrane (DM), lipid rafts (LR), endoplasmic reticulum (ER), and Golgi apparatus (GA). The results provide insights into the general properties of site-specific signaling networks and also into specific mechanisms that link biochemical processes such as TP53 and ERK signaling with distinct biological effects.

RESULTS

Mapping the Compartmentalized HRAS Interactome

We established HeLa cell lines stably expressing HRASV12 constructs that are either native or directed to the DM, LR, ER, or GA (Figure S1) by specific localization signals (Matallanas et al., 2006). A Flag tag allows to immune-purify and identify proteins binding to HRASV12 under steady-state conditions at the different subcellular sites by quantitative mass spectrometry (qMS) (Turriziani et al., 2014). Using a multistage analysis pipeline, which considers known PPIs and three-dimensional (3D) structural data (Figure 1A), we identified 397 HRASV12 interactors across all localizations (Figures 1B and 1C; Table S1). They contain ~20% of known RAS interactors, such as RAF1, RGL3, and RIN1, and 341 new interactors (Table S1).

Interestingly, the number of HRASV12 interactors differed between subcellular localizations (Figure 1C). Only ~5% of interactions occurred at all localizations, while ~53% were specific to individual locations (Figure 1D). ER had the most (231) binders, followed by the DM (155). Pathway enrichment analysis (Figure 1E; Table S1) showed that the interactome of untargeted HRAS engaged the classic RAS effector pathways, suggesting that it covers most of the known aspects of HRAS signaling. Examples include receptor tyrosine kinase (RTK) and G-protein coupled receptor (GPCR) pathways that are regulated from most localizations. In addition, the interactome analysis indicated that HRASV12 regulates biosynthetic and metabolic pathways mainly from the ER and immune signaling mainly from the GA. These pathways are outside of the classic HRAS signaling repertoire but are increasingly recognized as key contributors to HRAS transformation. HRAS is involved in immune cell signaling (Johnson and Chen, 2012) and in regulating immune cell infiltration in tumors (Thorsson et al., 2018). Mutant HRAS also profoundly influences metabolism harmonizing glycolysis and oxidative phosphorylation with biosynthetic pathways to enable sustained proliferation (Chesney and Telang, 2013). Especially lipid biosynthetic pathways were enriched, which is intriguing in light of a recent report that mice expressing mutant HRAS have severe aberrations in lipid metabolism (Oba et al., 2018). These results indicate that HRASV12 signaling is more diversified than previously thought and that differential subcellular localization may contribute to this diversification.

Mapping the Compartmentalized HRAS-Regulated Phosphoproteome

To expand the pathway analysis further downstream, we assayed global phosphoproteome changes induced by HRAS signaling from different subcellular compartments. While for the interaction proteomics it was inevitable to use exogenously expressed HRASV12, for the phosphoproteomics we directed the catalytic CDC25 domain of the RASGRF1 guanine nucleotide exchange factor (GEF) to the different subcellular localizations (Figure S2A). HeLa cell lines stably expressing these constructs activate endogenous HRAS selectively at the targeted sites (Herrero et al., 2018).

Phosphopeptides were enriched by an IMAC-Ti^{4+} protocol (Zhou et al., 2013) and analyzed by qMS identifying 7,469 unique phosphosites (Table S2). We developed an analysis pipeline that assesses changes in phosphorylation sites and reconstructs kinase-substrate networks (Figure 2A). Our kinase-substrate reconstruction algorithm is highly accurate when benchmarked

Figure 1. HRASV12 Interactomes at Different Subcellular Localizations

(A) Workflow and data analysis pipeline for determining HRASV12 interactomes at different subcellular localizations. DM, disordered membrane; GA, Golgi apparatus; LR, lipid rafts; ER, endoplasmic reticulum; CTRL, empty vector.

(B) Classification of HRASV12 interactors according to GO terms. Proteins are represented by ellipses with size indicating how likely a protein directly interacts with HRASV12. GO categories are in the same color. NA, not applicable, i.e., this cluster did not have a dominant GO term.

(C) Number of HRAS interactors at different subcellular localizations. TOT, untargeted HRASV12. See Table S1 for a full list of interactors.

(D) Venn diagram depicting overlap of HRASV12 interactomes at different subcellular sites.

(E) Heatmap of enriched pathways induced by HRASV12 interactors at different subcellular localizations. Biosynthetic and metabolic pathways are highlighted in green, immune signaling in yellow, and RTK and GPCR pathways in gray.

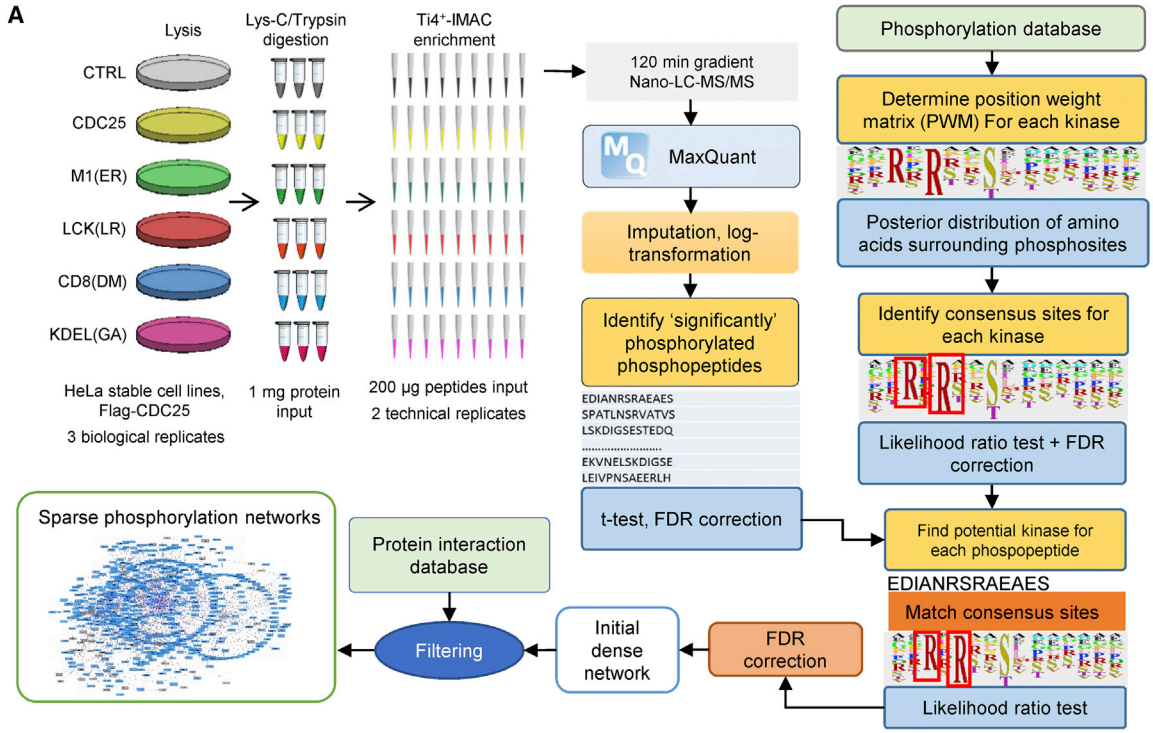

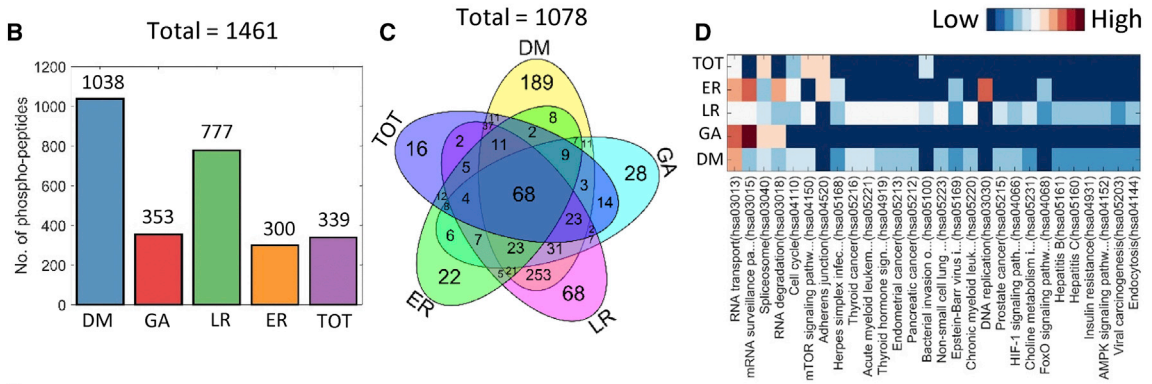

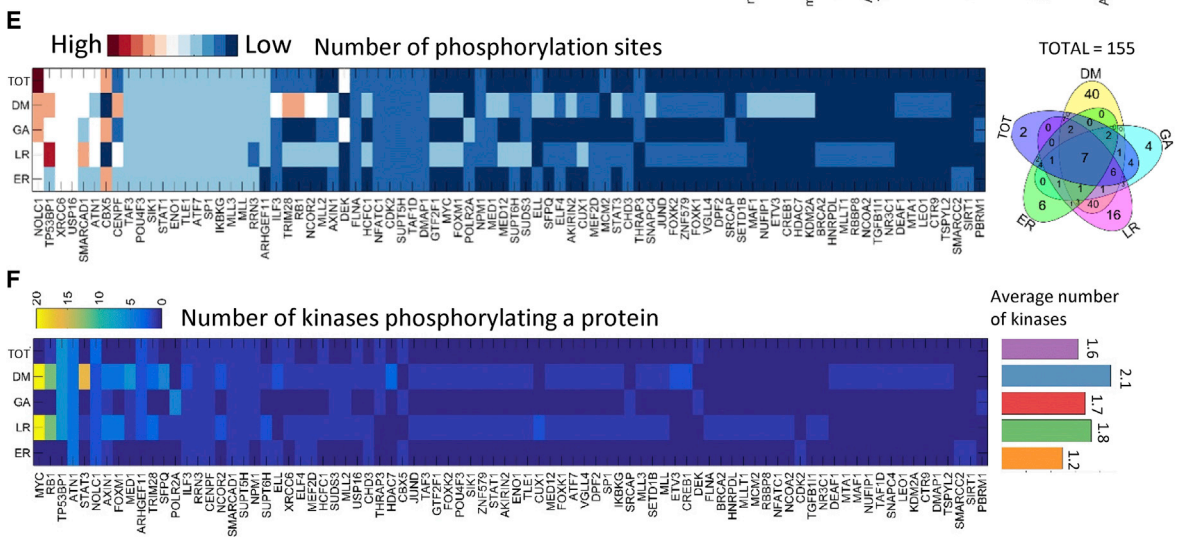

(legend on next page)

against experimental data and commonly used prediction software (Figure S2B; Table S2). 1,461 phosphosites, belonging to 1,078 unique proteins, were differentially phosphorylated with 74% of HRAS-induced phosphosites activated at the LR and DM (Figure 2B). Only ~6% of all phosphosites were independent of HRAS localizations (Figure 2C). Thus, while most HRAS PPIs occur at the ER and DM, HRAS stimulates phosphorylation and downstream pathways mainly when signaling from the cell membrane (Figure 2D; Table S2). Some of the classic RAS-dependent pathways, such as RTK signaling, identified in the HRASV12 interactome were also enriched in the phosphoproteome. Moreover, general cancer pathways and pathways for bladder, thyroid, endometrial, prostate, and non-small cell lung cancer were enriched in both interactome and phosphoproteome, suggesting that transforming HRAS functions are initiated in HRAS signaling complexes and propagated through phosphorylation networks. The phosphoproteome featured more signaling pathways, e.g., WNT, MAPK, HIPPO, insulin, and transcriptional pathways, such as FOXO and HIF1 (Table S2). These results indicate that PPIs impinge more on local modulatory functions, while the phosphoproteome better reflects functional interactions that exert long-range control through modifying the function of signaling pathways and transcriptional regulators.

Signaling pathways affect gene expression by changing the activity of transcriptional regulators and TFs, primarily by phosphorylating them. Only ~5% of all TFs were phosphorylated independently of HRAS' subcellular localizations (Figure 2E), suggesting that transcriptional regulation exerted by phosphorylation is highly reliant on HRAS localization, preferentially on HRAS being activated at the cell membrane. Most TFs were phosphorylated by few kinases but on multiple sites (Figure 2E). Interestingly, MYC, STAT3, and RB1 were phosphorylated by >10 kinases activated by HRAS from the cell membrane (Figure 2F). These TFs are key regulators of cell proliferation, differentiation, and apoptosis (Gabay et al., 2014; Munoz et al., 2014; Rubin, 2013), and their phosphorylation by many kinases is consistent with pivotal functions as signal integrators for oncogenic transformation.

These results suggest that the HRAS interactomes at the cell membrane induce phosphorylation-mediated signaling more efficiently than the larger interactome at the ER. Additionally, HRAS regulates many TFs in a distributive manner through different kinase pathways emanating from different subcellular localizations. However, many kinase pathways activated by HRAS from the cell membrane converge on a few TFs that control biological functions deregulated in transformed cells.

Mapping the Compartmentalized HRAS-Regulated Transcriptome

As the kinase-substrate network analysis indicated that TFs are differentially regulated by HRAS localization-specific signaling, we surveyed global gene expression (Figure 3A). We developed an analysis pipeline (detailed in the STAR Methods) to identify genes that were differentially expressed depending on HRASV12 subcellular location and the TFs that regulate these genes (Table S3). The resulting transcriptional regulatory network (TRN) uses prior knowledge about gene expression regulation and links TFs to experimentally measured data using a Bayesian statistical framework (Santra, 2016). Briefly, the method uses chromatin immunoprecipitation (ChIP) data to determine direct TF-DNA interactions, PPIs to infer potential transcriptional complexes formed between them and other TFs, and gene ontology (GO) annotations to define whether these TF complexes and regulated genes share common functions. From this information, we derived a prior weighting score for the TRN model that subsequently was updated by experimental data (Santra, 2016).

As previously observed in NIH 3T3 mouse fibroblasts (Agudo-Ibáñez et al., 2007), most genes were regulated by HRASV12 signaling from the ER, while transcriptional changes triggered by HRASV12 at the LR and DM were modest (Figure 3B). This was unexpected as HRAS signaling from the cell membrane affected many TFs (Figures 2E and 2F). This discrepancy may be due to epigenetics. Negative regulation of gene expression via epigenetic mechanisms was a selectively enriched GO term when HRASV12 was at the DM (Table S3). Of the six genes matching this GO term, two were upregulated (DNMT1, PHF19) and five were downregulated (HIST1H3A, HIST2H3A, H1F0, H3F3A, CREBZF). DNMT1 is a DNA methylase that contributes to promoter silencing; PHF1 is part of the PRC2 polycomb complex that mediates transcriptional repression; HIST1H3A and HIST2H3A are histone species that are targets of posttranslational modifications regulating transcription; H1F0 is a histone that links nucleosomes; H3F3A is associated with transcriptionally active chromatin; and CREBZF is a TF that can strongly stimulate transcription. This pattern of regulation is consistent with a general transcriptional repression observed when HRASV12 signals from the DM. Few genes were regulated by HRASV12 from all locations, suggesting HRASV12-mediated transcriptomic changes are dependent on its localization (Figure 3C). Surprisingly, the untargeted HRASV12, despite influencing a small number of genes, PPIs, and phosphorylation sites, had the highest GO term enrichment (Figure 3D; Table S3). GO terms related to astrocyte activation, amyloid fibril formation, and neuronal differentiation were exclusively enriched for untargeted HRASV12. These findings are

Figure 2. HRAS-Induced Phosphoproteome at Different Subcellular Localizations

(A) Workflow and data analysis pipeline for phosphoproteomics. DM, disordered membrane; GA, Golgi apparatus; LR, lipid rafts; ER, endoplasmic reticulum; CTRL, empty vector.

(B) Number of phosphopeptides induced by HRAS activated at different subcellular localizations compared to the empty vector control. TOT, untargeted CDC25.

(C) Overlap of phosphorylated proteins induced by activating HRAS at different subcellular sites. See Table S1 for a full list of phosphosites.

(D) Heatmap showing KEGG pathway enrichment analysis.

(E) Localization-dependent phosphorylation of transcriptional regulators and transcription factors (TFs). The number of phosphorylation sites per protein is shown as heatmap and Venn diagram.

(F) Combinatorial phosphorylations of TFs. The heatmap shows the number of different kinases targeting a TF.

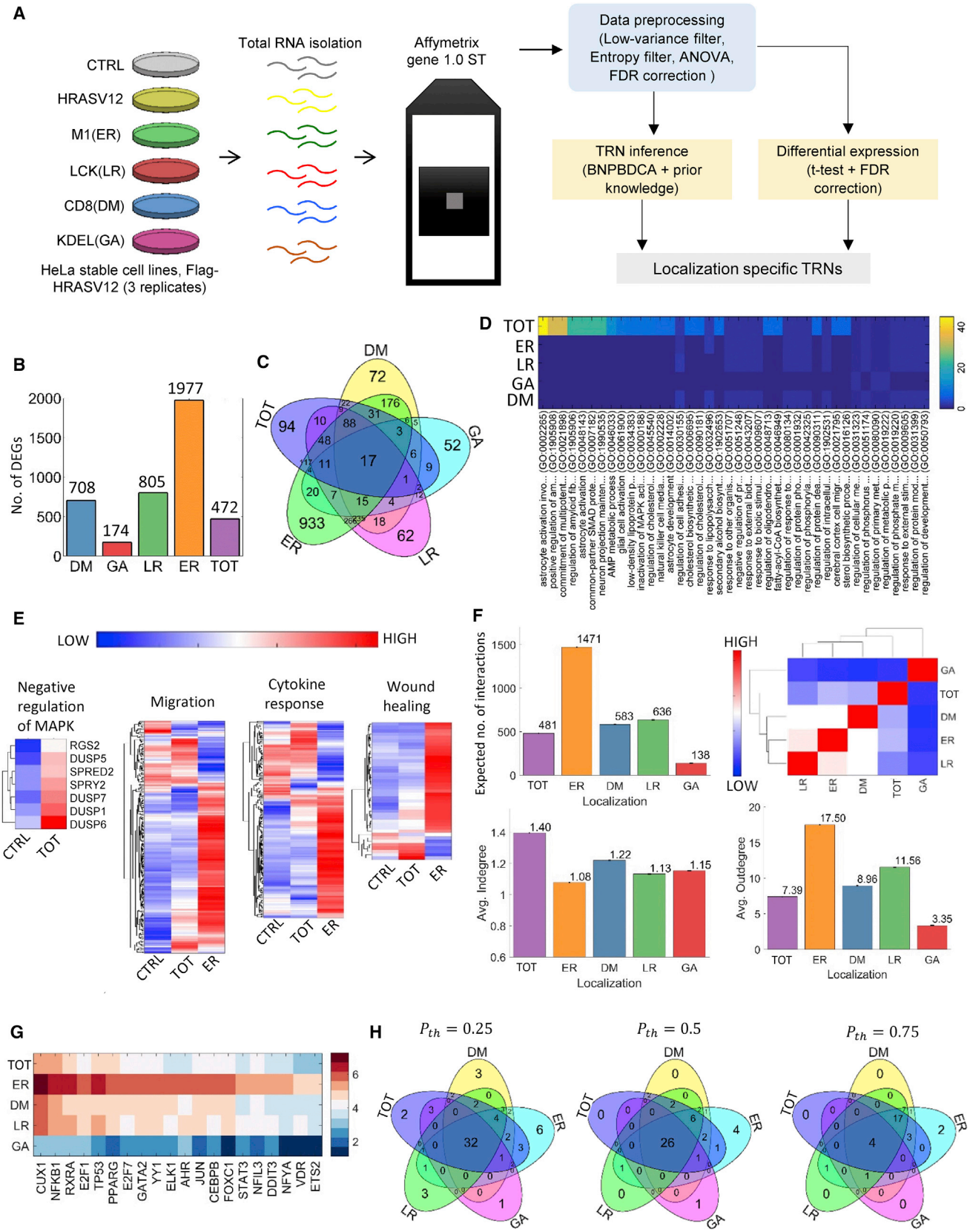

(legend on next page)

consistent with important roles of RAS in neuronal development (Zhong, 2016), the survival and activation of astrocytes (Haroon et al., 2011; Koseoglu et al., 2016), and the generation of β-amyloid (Amigoni et al., 2011). This result suggests either that the biological processes related to these GO terms require signaling from multiple subcellular compartments or that they are regulated from another compartment that is not covered by our targeted constructs. Moreover, the negative regulation of MAPK signaling exerted exclusively by untargeted HRASV12 may explain why relatively little signaling activity of untargeted HRAS was observed in our interaction and phosphoproteomic screens. Supporting this hypothesis, negative regulators of MAPK signaling (DUSP1/5/6/7, RGS2, SPRED2, SPRY2) were transcriptionally induced specifically by untargeted HRASV12 (Figure 3E). Interestingly, GO terms and corresponding genes related to cytokine response, wound healing, and cell migration were enriched among genes induced by HRASV12 located at the ER (Table S3; Figure 3E). As the cells are stably transfected, these changes represent steady-state HRAS signaling.

Reconstructing localization-specific TRNs revealed further details about the role of HRASV12 localization in transcriptional regulation (Figure 3F). Genes regulated by HRASV12 from the ER had 2.3 to 3 times more transcriptional interactions than genes controlled from other locations, but >10 times more interactions than GA-regulated genes. Additionally, the TRNs controlled by HRASV12 from the ER, LR, and DM shared similarities but were different to those induced from the GA. Interestingly, genes regulated by untargeted HRASV12 had the highest average in-degree (measuring how many TFs regulate a particular gene), indicating that these genes feature combinatorial regulation. By contrast, the out-degree (representing how many genes are regulated by a TF) was highest when HRASV12 was at the ER, explaining why so many genes are regulated from the ER. The CUX1 TF regulated the highest number of genes, followed by NFKB1, RXRA, and TP53, mainly when HRASV12 signaled from the ER (Figure 3G). CUX1 is overexpressed in many cancers and associated with tumor progression (Ramdzan and Nepveu, 2014). CUX1 protects mutant RAS cancers from oxidative DNA damage (Ramdzan et al., 2014), suggesting a pivotal role that enables the survival and expansion of RAS-transformed cells.

Interestingly, the TFs that make up site-specific TRNs are largely the same (Figure 3H), suggesting that the diversification of TRNs regulated from different subcellular sites results from the differential modulation of a shared set of TFs rather than from different TFs. This modulation seems to be exerted by differential, site-specific phosphorylation (Figures 2E and 2F).

Reconstruction of Multi-level HRAS-Regulated Site-Specific Signaling Networks

While each omic dataset provided interesting insights into localization-specific signaling, it was desirable to have a connected view, where all datasets are integrated into one network. Therefore, we developed a computational framework, MiNETi, to integrate the individual networks into a joined-up network. MiNETi is based on the principle that nodes belonging to different networks can be connected by empirical or logical rules. For instance, we know that kinases bind to their substrates and that phosphorylation can change protein function. Thus, a kinase that interacts with a TF is likely to phosphorylate this TF, which likely will change its function as measured by changes in gene expression. Logically, it follows that the more an incoming signal changes the activity of this kinase, the more it will change the activity of the cognate TF. Thus, we can rank the performance of the chosen rules by comparing and updating them against the experimentally observed data. This is a flexible framework for data integration. However, it also is rigorous as every step is statistically controlled.

As a paradigm, we have used MiNETi to analyze signal processing from HRASV12 interactors at different peripheral membrane compartments to nuclear changes in gene transcription. Briefly, MiNETi starts with an empty network. Then, for each subcellular localization of HRASV12, MiNETi adds (1) known PPIs between HRAS and the proteins identified in the MS interactome screens; (2) known PPIs among proteins in the HRAS interactome; (3) known PPIs between proteins in the HRASV12 interactome and the kinases of the corresponding phosphorylation networks; (4) all kinase-substrate interactions in the reconstructed phosphorylation network; (5) known PPIs among the kinases of the phosphorylation networks; (6) known PPIs among RAS interactors and the TFs of the corresponding TRN; (7) known PPIs between localization-specific kinases, phosphoproteins, and TFs of the corresponding TRNs; and (8) the TRNs themselves (Figure 4; Table S4).

The resulting site-specific signaling networks (SSSNs; Figure 4) are mixed graphs containing undirected edges representing PPIs and directed edges representing kinase-substrate relationships and transcriptional regulations. Interactions in the

Figure 3. HRASV12 Subcellular Localization-Dependent Transcriptome

(A) Workflow and data analysis pipeline for determining transcription regulatory networks (TRNs) driven by HRASV12 from different subcellular sites. DM, disordered membrane; GA, Golgi apparatus; LR, lipid rafts; ER, endoplasmic reticulum; CTRL, empty vector.

(B) Numbers of differentially expressed genes when HRASV12 signals from different subcellular sites. TOT, untargeted HRASV12. See Table S3 for a full list of genes.

(C) Venn diagram showing the overlap between gene expressions regulated by HRASV12 signaling from different locations.

(D) The top 40 enriched GO terms in transcriptomes regulated by different HRASV12 localizations.

(E) Hierarchical agglomerative clustering of differentially expressed genes associated with selected functions.

(F) HRASV12 localization-specific TRN characteristics. Top left panel: the expected number of interactions, which represents the accumulated probability that a TF regulates a gene. Top right: differences between HRASV12 localization-specific TRNs measured by the Pearson correlation between their interaction probabilities. Bottom left: average in-degrees of genes regulated by HRAS from different locations. Bottom right: average out-degrees (AODs).

(G) Compartment-specific AODs of 20 TFs with the largest numbers of regulated genes (log2 scale).

(H) Comparison of TFs regulating the genes influenced by HRASV12 from different subcellular locations, performed for three different thresholds (P_{th} = 0.25, 0.50, 0.75) of interaction probabilities.

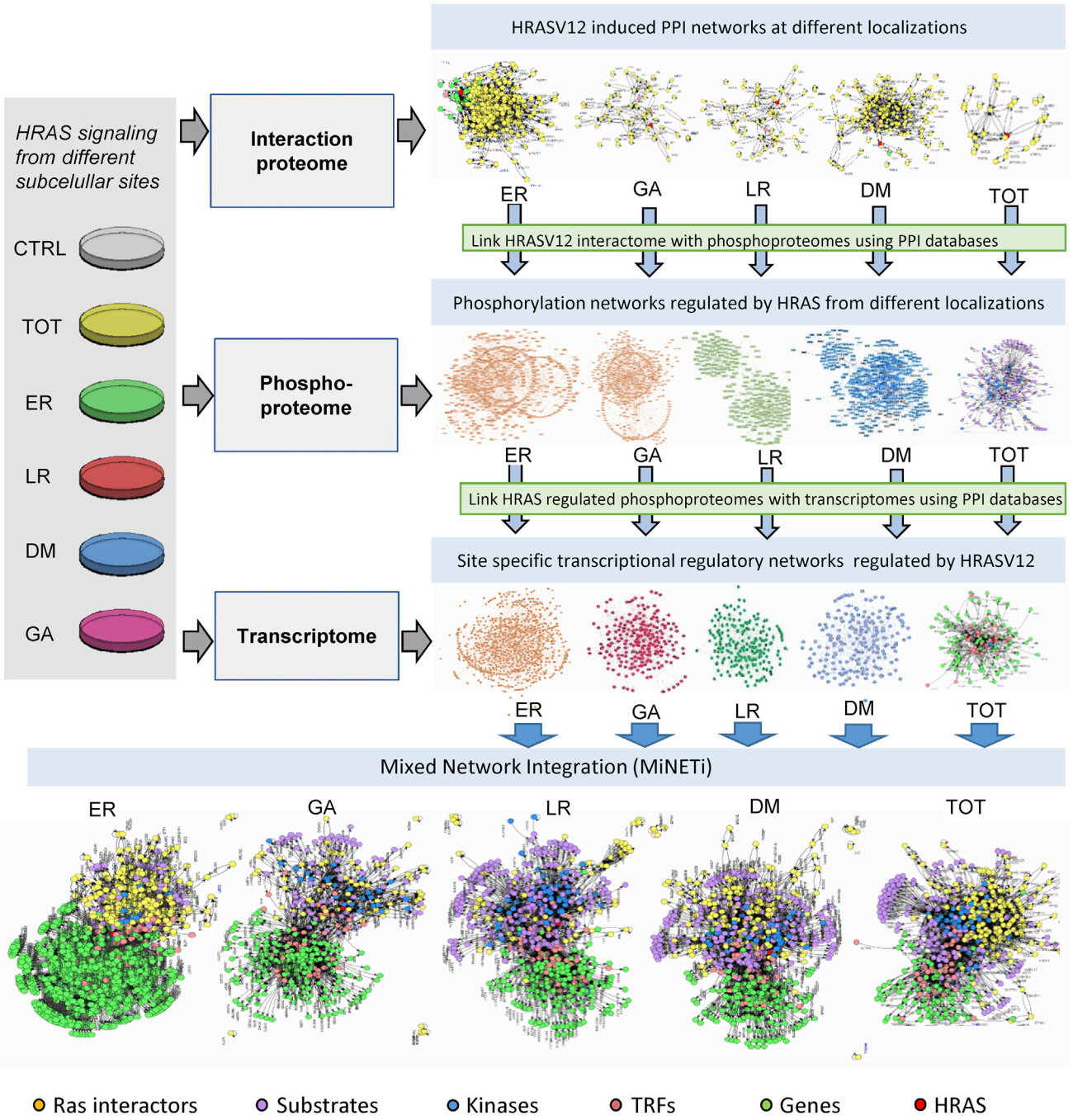

Figure 4. Reconstruction of Multi-level HRAS Signaling Networks by Integrating Heterogeneous Omics Data
See text and STAR Methods for details.

integrated networks are annotated, i.e., PPIs detected in the MS interactome screens, PPIs that were used to link HRAS interactomes with phospho-proteome and transcriptome, kinase-substrate interactions inferred from the phosphoproteomic data, or transcriptional interactions inferred from the microarray data (Table S4). In order to investigate the peripheral pathways contributing to the reconstructed SSSNs, we performed pathway enrichment analysis of the subnetworks that consisted of PPI and kinase-substrate interactions (Figure 5; Table S5). HRAS regulates a large variety of pathways from different subcellular sites. Although most pathways were regulated from all sites, some were enriched when HRAS signaled from the DM or LR. These included MAPK, TRK (neurotrophin), and ERBB signaling, where RAS has a known essential role but also

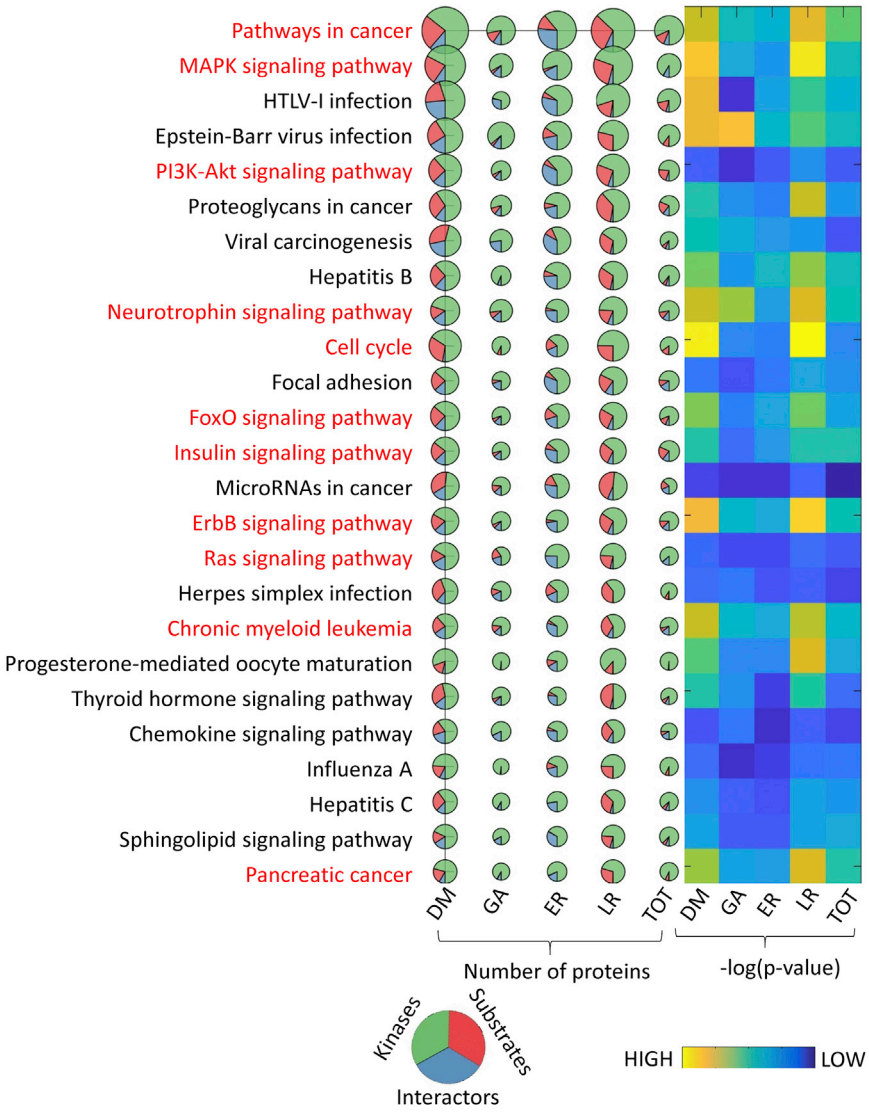

Figure 5. Comparison of Pathways Regulated by HRAS from Different Subcellular Localizations

Pathway enrichment analysis of HRASV12 interactors, predicted kinases, and substrates. Pathways are shown on the y axis, and HRAS locations are on the x axis. Pathways where RAS has known critical roles are highlighted in red. Pie charts represent how many components of a pathway correspond to HRAS interactors (blue), predicted kinases (green), and substrates (red). Pie chart sizes are proportional to the number of pathway components identified. The heatmap shows pathway enrichment scores (−log(p values)). DM, disordered membrane; GA, Golgi apparatus; LR, lipid rafts; ER, endoplasmic reticulum; TOT, untargeted HRASV12 (interactors) or untargeted CDC25 (kinases, substrates). Also see Table S5.

pathways linked to the cell cycle, pancreatic cancer, chronic myeloid leukemia, and cancer pathways in general. These results confirm the key role RAS plays in human cancers, underlining its crucial role in chronic myeloid leukemia (Million and Van Etten, 2000) and pancreatic cancer (Hobbs et al., 2016). In terms of components, the top 10 most enriched pathways included MAPK, PI3K/AKT, TRK, cancer pathways, and cell cycle signaling. While the former participate in known RAS effector pathways, the role of RAS in the cell cycle is less clear. A main function of RAS is to overcome the G1/S checkpoint by inactivating the RB1 and TP53 tumor suppressor proteins (Drosten et al., 2014). However, cells progressing from the G1 phase to the S phase require RAS signaling throughout the G1 phase (Rose et al., 1998), indicating that other RAS effectors are involved. Our study suggests that these effectors are mainly regulated by HRAS signaling from the cell membrane. Interestingly, many pathways that are not typically associated with RAS were also enriched, especially pathways associated with infections by tumorigenic viruses, such as Epstein-Barr, human T-cell leukemia virus type 1 (HTLV-1), and hepatitis B/C. These results indicate a potential role of RAS in human viral carcinogenesis that should be further explored.

SSSNs and Known RAS Effector Pathways

As RAS signaling is well characterized, we compared our results to existing knowledge (Figure S3A). Many components of these known pathways were identified in our interactome and phosphoproteomic screens. While the majority of HRASV12 interactors were found at the ER, the strongest phosphorylations were observed when HRAS was signaling from the DM, followed by LR (Figure S3B). Interestingly, both RAF1 and its substrate MAP2K2 (MEK2) were enriched in ER-associated HRASV12 interactors, but their phosphorylation was regulated from the cell membrane. The site-specific MEK2 phosphorylation was related to preventing MEK2 from activating AKT (Procaccia et al., 2017), suggesting that the cell membrane is not only responsible for the activation of the MEK-ERK pathway but also for limiting its crosstalk to other pathways. Similarly, PPP1R12A (MYPT1), a phosphatase that regulates myosin light chain kinase and smooth muscle contraction, was enriched in the ER-specific interactome but phosphorylated from the DM at an inhibitory site (Zagórska et al., 2010). Another example for localization-specific antagonism is cell cycle regulation. The inactivating phosphorylation of RB1, which is prerequisite for cell cycle entry (Rubin, 2013), was stimulated mainly from the DM, while the ER mediated the inhibitory phosphorylation of CDK2, which prevents cell cycle progression (Welburn et al., 2007).

These observations indicate that site-specific HRAS signaling may orchestrate critical cellular processes. Therefore, we assessed the contribution of SSSN components to the overall

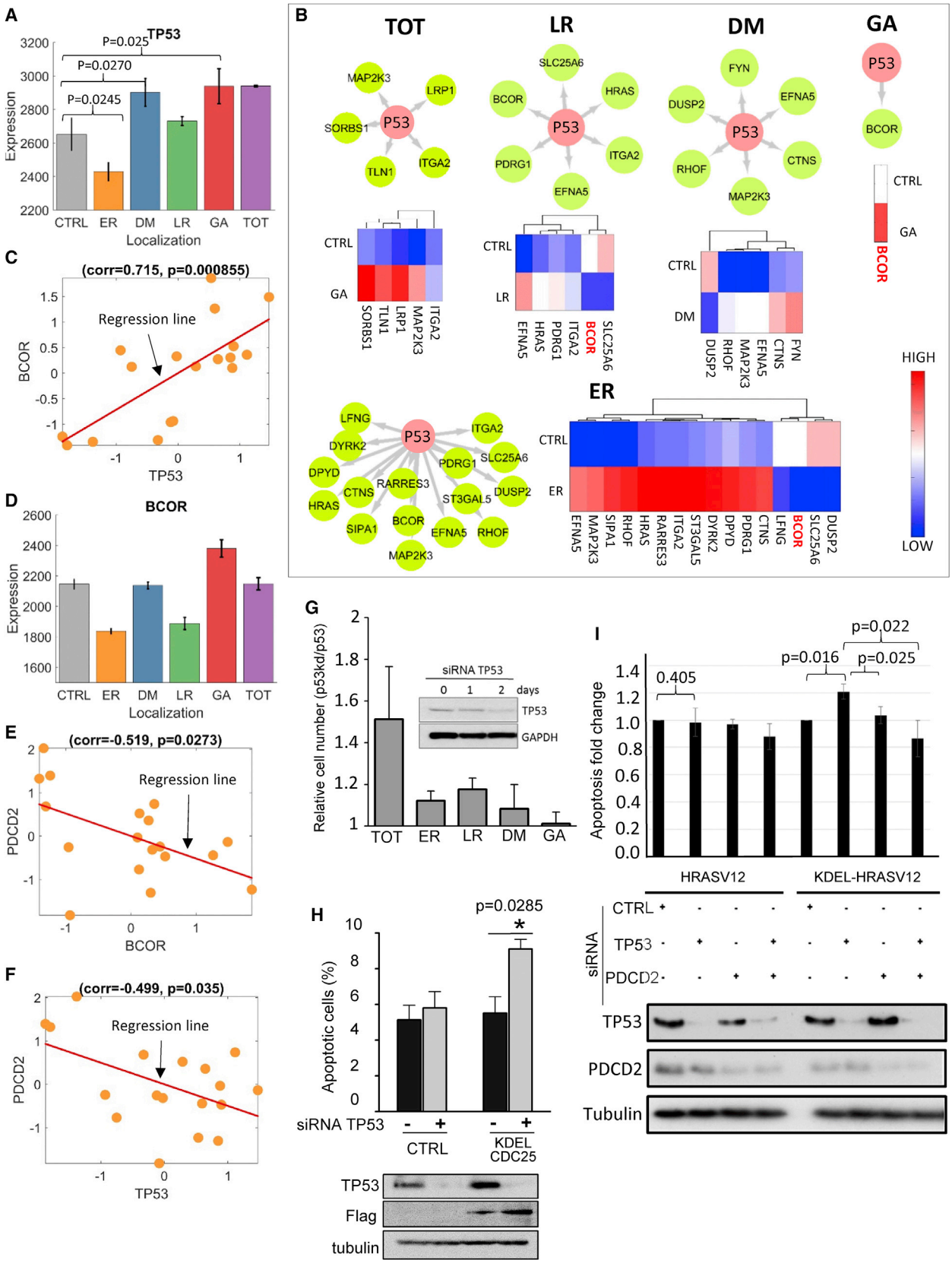

(legend on next page)

signaling capacity by summing up the number of interactions they participate in. Most proteins showed the highest capacity when HRAS signaled from the DM, followed by the LR, reflecting patterns seen in the phosphoproteomic screens (Figure S3C). The site-specific signaling capacities were superimposed on known RAS effector pathways and linked to their biological outputs based on GO enrichment of the corresponding transcriptomic data (Figures S3D–S3H). This provided an intuitive way of visualizing the differential regulation of biological processes by HRAS from different subcellular localizations. Pathway signaling capacities were calculated by summing up the signaling capacities of their components (Figure S3I). This analysis confirmed the results shown in Figure 5, i.e., that HRAS regulates most of its effector pathways from the DM and LR, while little signaling occurs from the GA. For some pathways, e.g., ERK and AKT, this behavior largely agrees with previous experimental results (Casar et al., 2009; Matallanas et al., 2006). Exceptions are cell cycle and RAC/PAK pathways, which had the highest activity when HRAS was at the ER. These observations agree with previous studies that showed that ER dysfunction causes rapid, HRAS-mediated cell-cycle arrest (Denoyelle et al., 2006) and that RasGRF1 co-localizes with HRAS in the ER, but not the PM, and activates both HRAS and RAC1 (Arozarena et al., 2004).

Differential Specification of TP53 Effects

The tumor suppressor TP53 mRNA expression was significantly affected by HRASV12 localization. It was underexpressed when HRASV12 was at the ER, but overexpressed when HRASV12 was at the DM and GA (Figure 6A). To determine which phenotypes might be controlled by site-specific HRAS regulation of TP53, we focused on TP53's most likely (interaction probability > 0.75) transcriptional targets. Many of them showed HRASV12 localization-specific expression (Figure 6B), but the BCL6 co-repressor (BCOR) was the only TP53 target gene that was overexpressed when HRASV12 was at the GA. BCOR mRNA expression positively correlated with TP53 expression (Figures 6C and 6D), suggesting that it is transcriptionally regulated by TP53. BCOR binds to BCL6 (Huynh et al., 2000) and potentiates BCL6-mediated transcriptional repression of Programmed Cell Death 2 (PDCD2) (Baron et al., 2007), which induces apoptosis by activating caspases (Baron et al., 2010). Indeed, PDCD2 expression was negatively correlated with BCOR and TP53 expression (Figures 6E and 6F), suggesting that TP53 may indirectly inhibit PDCD2, and thereby apoptosis, by activating BCOR. As both TP53 and BCOR were overexpressed when HRASV12 was at the GA, we expected this potential anti-apoptotic function of TP53 to be linked to GA-specific HRAS signaling.

To test this hypothesis, we knocked down TP53 in HeLa cells stably expressing CDC25 at different subcellular localizations and measured apoptosis and proliferation. Although HeLa express a HPV18 E6 protein that enhances TP53 degradation, TP53 expressed in HeLa cells retains both its nuclear and non-nuclear functions (Chipuk et al., 2004; Hoppe-Seyler and Butz, 1993). In our HeLa cells, the TP53 protein was readily detectable, and TP53 knockdown slightly increased proliferation in all conditions except when CDC25 was at the GA (Figure 6G). Vice versa, TP53 knockdown reduced apoptosis in vector control cells and cells expressing CDC25 targeted to the cell membrane. However, when HRAS was activated at the GA and to a lesser extent at the ER, TP53 knockdown increased apoptosis (Figure S4). Consistent results were obtained using a different apoptosis assay (Figure 6H). To assess whether PDCD2 plays a role in TP53-mediated survival, we measured apoptosis after knocking down TP53 and PDCD2 individually and in combination. PDCD2 knockdown neutralized the TP53 knockdown-mediated increase in apoptosis in KDEL-HRASV12 (GA) cells but not in HRASV12 cells, confirming that TP53 can protect cells from apoptosis through suppressing PDCD2 expression when HRAS signals from the GA.

Migration Is Controlled by HRAS Signaling from the ER

HRASV12 targeted to the ER strongly induced cell-migration-related genes (Figure 3E; Table S6), and GO enrichment analysis showed that HRASV12 signaling from the ER accounted for most of the migration-related gene expression (Figure 7A) suggesting that migration is likely controlled by HRAS from the ER.

Figure 6. HRAS Signaling from the GA Enhances Cell Survival via p53

(A) HRASV12 localization-specific expression of TP53 mRNA. DM, disordered membrane; GA, Golgi apparatus; LR, lipid rafts; ER, endoplasmic reticulum; TOT, untargeted HRASV12; CTRL, empty vector. Results represent 3 independent replicates; y axis shows gene expression as log 2 intensity values; error bars are SEM; and p values were calculated by t test.

(B) HRASV12 localization-specific mRNA expression of high probability (>0.75) transcriptional targets of p53.

(C) Correlation between TP53 versus BCOR mRNA expression calculated by Pearson linear regression. x and y axis, standardized expression values.

(D) HRASV12 localization-specific BCOR mRNA expression. Results represent 3 independent replicates; y axis shows gene expression as log 2 intensity values; error bars are SEM; and p values were calculated by t test.

(E and F) Correlations between PDCD2 versus BCOR and TP53 mRNA expression calculated by Pearson linear regression. x and y axis, standardized expression values.

(G) Proliferation of cells expressing targeted CDC25 constructs following TP53 knockdown. Data represent the fold-change in cell numbers measured 2 days after transfection with TP53 small interfering RNA (siRNA) versus non-targeting control siRNA. Western blot shows downregulation of TP53 protein. DM, disordered membrane; GA, Golgi apparatus; LR, lipid rafts; ER, endoplasmic reticulum; TOT, untargeted CDC25; TP53kd, TP53 knockdown. Data represent 2 independent experiments; error bars indicate SEM.

(H) HeLa cells stably expressing CDC25 at the GA (KDEL-CDC25) were transfected with 60 pmol TP53 targeting siRNA (+) and a non-targeting siRNA (–). Apoptosis was measured by assessing DNA fragmentation in cells serum starved for 32 h. The results represent 3 independent experiments; error bars are SEM; and p values were calculated using the t test. Western blots show downregulation of p53 protein and expression of Flag-tagged KDEL-CDC25.

(I) Apoptosis in response to TP53 and PDCD2 knockdowns in HeLa cells transfected with HRASV12 and HRASV12 targeted to the GA (KDEL-HRASV12). Apoptosis was measured as in (H). The results represent 3 independent experiments, error bars are SEM, and p values were calculated by t test. Western blot shows downregulation of TP53 and PDCD2 proteins.

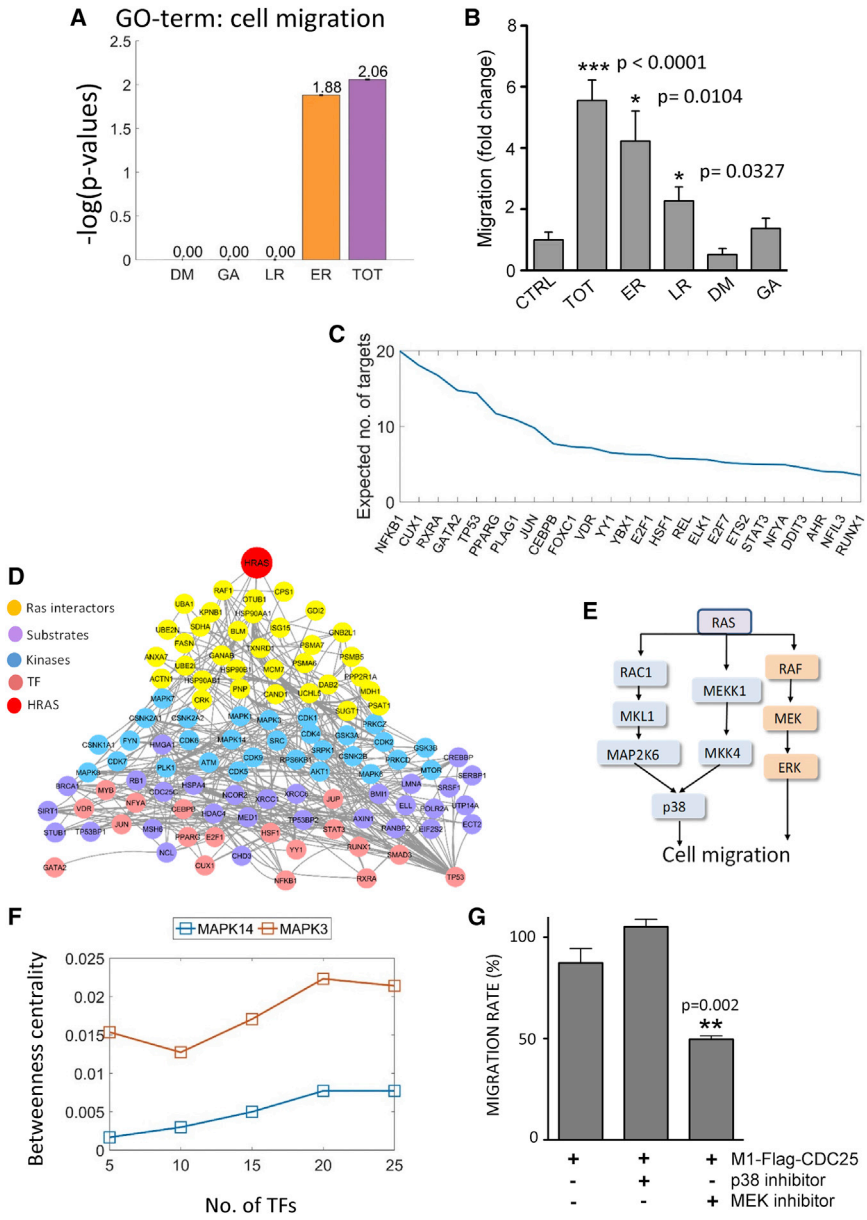

Figure 7. HRAS Regulates Migration from the ER

(A) Enrichment of the GO term "cell migration" among genes differentially expressed upon HRASV12 signaling from specific subcellular locations. DM, disordered membrane; GA, Golgi apparatus; LR, lipid rafts; ER, endoplasmic reticulum; TOT, untargeted HRASV12. Also see Table S6.

(B) Experimental quantification of cell migration. DM, disordered membrane; GA, Golgi apparatus; LR, lipid rafts; ER, endoplasmic reticulum; TOT, untargeted CDC25; CTRL, empty vector. Results represent 2 independent experiments with 4 biological replicates each; error bars are SEM.

(C) Expected number (sum of interaction probabilities) of migration-related gene targets (y axis) for each TF (x axis).

(D) Signaling network connecting HRASV12 to the top scoring TFs in (C).

(E) Literature-based knowledge of RAS signaling pathways that regulate HeLa cell migration.

(F) Betweenness centralities of ERK2 (MAPK1) and p38α (MAPK14) in the signaling network connecting HRASV12 at the ER to different numbers of top-ranked TFs that regulate migration.

(G) The effect of p38 and MEK inhibitors on cell migration stimulated by activating endogenous HRAS at the ER (M1-Flag-CDC25). Results represent 2 independent experiments with 4 replicates each; error bars are SEM; and p values were calculated by t test.

Measuring the migration of HeLa cells stably expressing the CDC25 GEF at different compartments showed that only untargeted CDC25 and CDC25 at the ER efficiently stimulated migration (Figure 7B). Activation of endogenous HRAS at other compartments induced migration less efficiently. In order to rank the influence of TFs on the regulation of migration-related genes, we summed the probabilities of all interactions between TFs and migration-related genes (Figure 7C). Then, we tracked the signaling pathways connecting HRAS to the top five migration-regulating TFs in the SSSN that represents HRAS signaling from the ER (Figure 7D). Surprisingly, these pathways contain ERK but not p38 kinase, although both kinases were previously shown to be instrumental in HeLa cell migration (Sun et al., 2002) and are part of generic models of RAS-mediated migration (Figure 7E) (Huang et al., 2004). We performed the same analysis gradually, adding less influential TFs, three at a time, and assessed the network connectivity by calculating the betweenness centrality, i.e., the fraction of shortest paths from HRAS to TFs leading through a certain node (Figure 7F). Only ERK1 (MAPK3) appeared in the pathways connecting HRAS to the top three TFs. When additional, less influential, TFs were included, ERK2 (MAPK1), p38δ (MAPK13), and p38α (MAPK14) appeared in the pathways connecting these TFs to HRAS, but p38δ and p38α had significantly smaller betweenness centrality than ERK1/2. This analysis suggests that ERK is more important than p38 for cell migration stimulated by HRAS from the ER. Indeed, MEK inhibition significantly reduced migration, whereas p38 inhibition had no effect (Figure 7G), confirming the predictions of our integrated network analysis.

DISCUSSION

Rapid technological advances in omics methods have now shifted the bottleneck from data production to data interpretation and integration. Especially data integration is becoming critical. We have made great progress in analyzing individual omics

datasets and can reconstruct global networks of gene regulation, protein interactions, phosphorylations, other posttranslational modifications, and metabolism. Functionally, all these different networks work together to produce specific biological responses. Therefore, it is desirable to develop an integrative framework that provides a coherent view of how these networks interact and how these interactions specify biological responses. Such efforts are hampered by many reasons, including (1) different depths of coverage of the different omics technologies; (2) different timescales on which these networks operate; and (3) incompatibilities of data output formats from different omics methods. Thus, integration at the level of primary data becomes difficult. To overcome this hurdle, we have developed MiNETi based on the concept that diverse biochemical and biological networks can be integrated through empirical rules that describe connectivities between different networks. MiNETi is primarily a conceptual framework that combines an array of statistical tools to facilitate such connections.

Here, we used MiNETi to integrate proteomic interaction data, phosphoproteomics, and transcriptome data. These datasets are typical representatives of what modern biological studies generate. They also represent all of the challenges outlined above. The interactome, in this case of HRASV12, is small compared to the phosphoproteome, which, however, features many missing data. The transcriptome is genome wide and comprehensive but delayed in terms of timescale relative to protein interaction and phosphorylation events. The data formats and features of the resulting individual networks are also different. MiNETi uses a two-step approach to connect them. In the first step, it analyzes each type of data separately using statistical pipelines tailored to each type of data. Each of these pipelines combines experimental omic profiles with existing PPIs, proteins' 3D structural information, phosphorylation, kinase consensus motifs, TF-DNA binding, TF-TF binding, GO annotations, and other relevant prior information to reconstruct the corresponding individual networks in a manner enriched by biological knowledge. In the second step, the individual networks are integrated in one coherent network using biologically intuitive rules that connect nodes between the different networks, as follows: (1) the interactors of HRAS include potential regulators of the downstream phosphorylation network; (2) the phosphorylation network induced by HRAS includes kinase-substrate pairs, some of which are likely to influence the activities of TFs; (3) TFs regulate transcription; and (4) transcriptomic changes relate to the cell's phenotype. The integrated network is hybrid, i.e., it features many different types of interactions, such as PPIs, kinase-substrate, and TF-DNA interactions, the first of which are undirected, and the last two are directed interactions. Although MiNETi has no explicit provision for integrating spatiotemporal dynamics, sequential relationships can be introduced by formulating appropriate rules, e.g., that changes in gene expression depend on prior TF phosphorylation. Such rules also could be used to incorporate feedback loops, e.g., by making a connection between nodes conditional on another previous connection. We did not explicitly consider feedback loops as the experiments were performed with stably transfected cells where HRAS signaling is at steady-state equilibrium, where feedback loops operate chronically. However, applying perturbation experiments will enable the incorporation of feedback regulation into MiNETi. This is an interesting future extension as examining known ERK-mediated feedback loops showed that their specificity is determined by HRASV12 localization and the type of substrate (Figure S5).

An important characteristic of the integrated network is that it provided a more coherent picture of molecular events triggered by HRAS than was possible by any individual omic screen. For instance, kinases such as ERK and JNK and TFs such as TP53, which are known to be regulated by HRAS, were not directly detected in the proteomic screens, but their presence was predicted by the kinase-substrate and TRN reconstruction, and they play important roles in the integrated networks. Therefore, the SSSNs allow us to discover global properties of networks and to derive specific hypotheses about the detailed behavior of pathways and components that would not be possible based on the analysis of the individual omics networks. The capability of the MiNETi framework to seamlessly transition between the analysis of global features and specific predictions makes it very useful for the discovery of new biological phenomena in a context that also delivers initial mechanistic interpretation.

As a paradigm, we have applied MiNETi to decipher subcellular localization-specific HRAS signaling. While RAS signaling was thought to exclusively originate from the PM, increasing evidence showed that RAS signaling is highly compartmentalized (Arozarena et al., 2004; Bivona et al., 2003, 2006; Chiu et al., 2002; Daniels et al., 2006; Harding et al., 2005; Herrero et al., 2018; Inder et al., 2008; Jura et al., 2006; Lorentzen et al., 2010; Matallanas et al., 2006; Mor et al., 2007; Rocks et al., 2005). These studies clearly demonstrated that RAS can signal from different compartments and that this compartmentalization can specify different biological outcomes. An unresolved question is how RAS is activated at these different subcellular compartments. One possibility is the existence of localization-specific GEFs (Arozarena et al., 2004; Bivona et al., 2003), and another is that RAS is activated at the PM and then travels through different compartments as part of its re-localization cycle (Lorentzen et al., 2010). Regardless of how RAS is activated at different subcellular localizations, a main question is whether localization will change the biochemical and biological outcomes of RAS signaling. Our study addresses this point on a global level, showing that signaling pathways are rewired dependent on the subcellular origin of HRAS signals. Interestingly, much of the rewiring is due to dynamic changes in the affinities of HRAS binders and the differential triggering of downstream phosphorylation networks. This combination results in different TRNs that ultimately can specify different biological functions. In fact, this seems to be the case. Cell migration was mainly controlled by HRAS signaling from the ER to ERK. This control likely is exerted by the numerous cell-migration-related genes induced by HRAS at the ER (Figure 3E). Although the ER was implicated in migration (Chevet et al., 2015), a role for RAS was not previously identified. Similarly, TP53 is usually linked to promotion of apoptosis but also can protect cells when the apoptotic stress is mild (Kruiswijk et al., 2015). However, RAS activation is usually associated with TP53 phosphorylation on S15 and induction of apoptosis (Brown and

Benchimol, 2006). In our study, HRAS signaling from the cell membrane enhanced TP53-mediated apoptosis, while HRAS at the GA enhanced survival, and both functions cancelled each other out when HRAS was activated throughout the cell (Figure S4). Thus, TP53 may play a dual role in HRAS signaling with the biological outcome determined by the balance of compartmentalized HRAS activation. These examples show that integrated network analysis can facilitate the discovery of new biological functions and their validation.

STAR★METHODS

Detailed methods are provided in the online version of this paper and include the following:

- KEY RESOURCES TABLE
- CONTACT FOR REAGENT AND RESOURCE SHARING
- EXPERIMENTAL MODEL AND SUBJECT DETAILS
- METHOD DETAILS
  - Experimental Methods
- DATA ANALYSIS AND COMPUTATIONAL MODELS
  - Interactome analysis pipeline
  - Phosphoproteomics data analysis pipeline
  - Transcriptomic data analysis pipeline
  - Expected in- and out-degrees *(Figure 3F)*
  - Development of MiNETi
- QUANTIFICATION AND STATISTICAL ANALYSIS
- DATA AND SOFTWARE AVAILABILITY

SUPPLEMENTAL INFORMATION

Supplemental Information includes five figures, six tables, and one data file and can be found with this article online at https://doi.org/10.1016/j.celrep.2019.02.038.

ACKNOWLEDGMENTS

This work was supported by the Science Foundation Ireland grants 06/CE/B1129, 14/IA/2395, and 15_CDA_3495; Irish Cancer Society BREAST-PREDICT grant CCRC13GAL; and by the European Union FP7 grant 278568 "PRIME-XS." T.-T.A. and A.J.R.H. were supported by the Roadmap Initiative Proteins@Work (184.032.201) funded by the Netherlands Organisation for Scientific Research (NWO). P.C. was supported by grant SAF-2015 63638R (MINECO/FEDER, UE); by Centro de Investigación Biomédica en Red de Cáncer; and by Asociación Española Contra el Cáncer (AECC), grant GCB141423113.

AUTHOR CONTRIBUTIONS

T. Santra designed and implemented the MiNETi analysis, and L.F.I.-M. helped with the revisions; A.H., D.M., J.R., A.v.K., T.-T.A., F.C., and L.A.-I. carried out and analyzed the experiments; T. Schwarzl and D.H. did the bioinformatic analysis; D.M., P.C., and W.K. designed the study and wrote the paper.

DECLARATION OF INTERESTS

The authors declare no competing interests.

Received: July 16, 2018
Revised: December 16, 2018
Accepted: February 11, 2019
Published: March 12, 2019

REFERENCES

Agudo-Ibáñez, L., Núñez, F., Calvo, F., Berenjeno, I.M., Bustelo, X.R., and Crespo, P. (2007). Transcriptomal profiling of site-specific Ras signals. Cell. Signal. *19*, 2264–2276.

Amigoni, L., Ceriani, M., Belotti, F., Minopoli, G., and Martegani, E. (2011). Activation of amyloid precursor protein processing by growth factors is dependent on Ras GTPase activity. Neurochem. Res. *36*, 392–398.

Aran, V., and Prior, I.A. (2013). Compartmentalized Ras signaling differentially contributes to phenotypic outputs. Cell. Signal. *25*, 1748–1753.

Arozarena, I., Matallanas, D., Berciano, M.T., Sanz-Moreno, V., Calvo, F., Muñoz, M.T., Egea, G., Lafarga, M., and Crespo, P. (2004). Activation of H-Ras in the endoplasmic reticulum by the RasGRF family guanine nucleotide exchange factors. Mol. Cell. Biol. *24*, 1516–1530.

Baron, B.W., Zeleznik-Le, N., Baron, M.J., Theisler, C., Huo, D., Krasowski, M.D., Thirman, M.J., Baron, R.M., and Baron, J.M. (2007). Repression of the PDCD2 gene by BCL6 and the implications for the pathogenesis of human B and T cell lymphomas. Proc. Natl. Acad. Sci. USA *104*, 7449–7454.

Baron, B.W., Hyjek, E., Gladstone, B., Thirman, M.J., and Baron, J.M. (2010). PDCD2, a protein whose expression is repressed by BCL6, induces apoptosis in human cells by activation of the caspase cascade. Blood Cells Mol. Dis. *45*, 169–175.

Bivona, T.G., Pérez De Castro, I., Ahearn, I.M., Grana, T.M., Chiu, V.K., Lockyer, P.J., Cullen, P.J., Pellicer, A., Cox, A.D., and Philips, M.R. (2003). Phospholipase Cgamma activates Ras on the Golgi apparatus by means of RasGRP1. Nature *424*, 694–698.

Bivona, T.G., Quatela, S.E., Bodemann, B.O., Ahearn, I.M., Soskis, M.J., Mor, A., Miura, J., Wiener, H.H., Wright, L., Saba, S.G., et al. (2006). PKC regulates a farnesyl-electrostatic switch on K-Ras that promotes its association with Bcl-XL on mitochondria and induces apoptosis. Mol. Cell *21*, 481–493.

Brown, L., and Benchimol, S. (2006). The involvement of MAPK signaling pathways in determining the cellular response to p53 activation: cell cycle arrest or apoptosis. J. Biol. Chem. *281*, 3832–3840.

Casar, B., Arozarena, I., Sanz-Moreno, V., Pinto, A., Agudo-Ibáñez, L., Marais, R., Lewis, R.E., Berciano, M.T., and Crespo, P. (2009). Ras subcellular localization defines extracellular signal-regulated kinase 1 and 2 substrate specificity through distinct utilization of scaffold proteins. Mol. Cell. Biol. *29*, 1338–1353.

Chesney, J., and Telang, S. (2013). Regulation of glycolytic and mitochondrial metabolism by ras. Curr. Pharm. Biotechnol. *14*, 251–260.

Chevet, E., Hetz, C., and Samali, A. (2015). Endoplasmic reticulum stress-activated cell reprogramming in oncogenesis. Cancer Discov. *5*, 586–597.

Chipuk, J.E., Kuwana, T., Bouchier-Hayes, L., Droin, N.M., Newmeyer, D.D., Schuler, M., and Green, D.R. (2004). Direct activation of Bax by p53 mediates mitochondrial membrane permeabilization and apoptosis. Science *303*, 1010–1014.

Chiu, V.K., Bivona, T., Hach, A., Sajous, J.B., Silletti, J., Wiener, H., Johnson, R.L., 2nd, Cox, A.D., and Philips, M.R. (2002). Ras signalling on the endoplasmic reticulum and the Golgi. Nat. Cell Biol. *4*, 343–350.

Cox, J., and Mann, M. (2008). MaxQuant enables high peptide identification rates, individualized p.p.b.-range mass accuracies and proteome-wide protein quantification. Nat. Biotechnol. *26*, 1367–1372.

Cox, A.D., Fesik, S.W., Kimmelman, A.C., Luo, J., and Der, C.J. (2014). Drugging the undruggable RAS: Mission possible? Nat. Rev. Drug Discov. *13*, 828–851.

Daniels, M.A., Teixeiro, E., Gill, J., Hausmann, B., Roubaty, D., Holmberg, K., Werlen, G., Holländer, G.A., Gascoigne, N.R., and Palmer, E. (2006). Thymic selection threshold defined by compartmentalization of Ras/MAPK signalling. Nature *444*, 724–729.

Denoyelle, C., Abou-Rjaily, G., Bezrookove, V., Verhaegen, M., Johnson, T.M., Fullen, D.R., Pointer, J.N., Gruber, S.B., Su, L.D., Nikiforov, M.A., et al. (2006). Anti-oncogenic role of the endoplasmic reticulum differentially activated by mutations in the MAPK pathway. Nat. Cell Biol. *8*, 1053–1063.

Drosten, M., Sum, E.Y., Lechuga, C.G., Simón-Carrasco, L., Jacob, H.K., García-Medina, R., Huang, S., Beijersbergen, R.L., Bernards, R., and Barbacid, M. (2014). Loss of p53 induces cell proliferation via Ras-independent activation of the Raf/Mek/Erk signaling pathway. Proc. Natl. Acad. Sci. USA *111*, 15155–15160.

Frese, C.K., Altelaar, A.F., Hennrich, M.L., Nolting, D., Zeller, M., Griep-Raming, J., Heck, A.J., and Mohammed, S. (2011). Improved peptide identification by targeted fragmentation using CID, HCD and ETD on an LTQ-Orbitrap Velos. J. Proteome Res. *10*, 2377–2388.

Gabay, M., Li, Y., and Felsher, D.W. (2014). MYC activation is a hallmark of cancer initiation and maintenance. Cold Spring Harb. Perspect. Med. *4*, a014241.

Gibbs, D.L., Gralinski, L., Baric, R.S., and McWeeney, S.K. (2014). Multi-omic network signatures of disease. Front. Genet. *4*, 309.

Haider, S., and Pal, R. (2013). Integrated analysis of transcriptomic and proteomic data. Curr. Genomics *14*, 91–110.

Harding, A., Tian, T., Westbury, E., Frische, E., and Hancock, J.F. (2005). Subcellular localization determines MAP kinase signal output. Curr. Biol. *15*, 869–873.

Haroon, F., Drogemuller, K., Handel, U., Brunn, A., Reinhold, D., Nishanth, G., Mueller, W., Trautwein, C., Ernst, M., Deckert, M., et al. (2011). Gp130-dependent astrocytic survival is critical for the control of autoimmune central nervous system inflammation. J. Immunol. *186*, 6521–6531.

Herrero, A., Reis-Cardoso, M., Jiménez-Gómez, I., Doherty, C., Agudo-Ibañez, L., Pinto, A., Calvo, F., Kolch, W., Crespo, P., and Matallanas, D. (2018). Characterisation of HRas local signal transduction networks using engineered site-specific exchange factors. Small GTPases, 1–13.

Higdon, D.M. (1998). Auxiliary Variable Methods for Markov Chain Monte Carlo with Applications. J. Am. Stat. Assoc. *93*, 585–595.

Hobbs, G.A., Der, C.J., and Rossman, K.L. (2016). RAS isoforms and mutations in cancer at a glance. J. Cell Sci. *129*, 1287–1292.

Hoppe-Seyler, F., and Butz, K. (1993). Repression of endogenous p53 transactivation function in HeLa cervical carcinoma cells by human papillomavirus type 16 E6, human mdm-2, and mutant p53. J. Virol. *67*, 3111–3117.

Horn, H., Schoof, E.M., Kim, J., Robin, X., Miller, M.L., Diella, F., Palma, A., Cesareni, G., Jensen, L.J., and Linding, R. (2014). KinomeXplorer: an integrated platform for kinome biology studies. Nat. Methods *11*, 603–604.

Huang, C., Jacobson, K., and Schaller, M.D. (2004). MAP kinases and cell migration. J. Cell Sci. *117*, 4619–4628.

Huang, W., Sherman, B.T., and Lempicki, R.A. (2009a). Bioinformatics enrichment tools: paths toward the comprehensive functional analysis of large gene lists. Nucleic Acids Res. *37*, 1–13.

Huang, W., Sherman, B.T., and Lempicki, R.A. (2009b). Systematic and integrative analysis of large gene lists using DAVID bioinformatics resources. Nat. Protoc. *4*, 44–57.

Huang, S., Chaudhary, K., and Garmire, L.X. (2017). More Is Better: Recent Progress in Multi-Omics Data Integration Methods. Front. Genet. *8*, 84.

Huynh, K.D., Fischle, W., Verdin, E., and Bardwell, V.J. (2000). BCoR, a novel corepressor involved in BCL-6 repression. Genes Dev. *14*, 1810–1823.

Imielinski, M., Cha, S., Rejtar, T., Richardson, E.A., Karger, B.L., and Sgroi, D.C. (2012). Integrated proteomic, transcriptomic, and biological network analysis of breast carcinoma reveals molecular features of tumorigenesis and clinical relapse. Mol. Cell. Proteomics *11*, M111.014910.

Inder, K., Harding, A., Plowman, S.J., Philips, M.R., Parton, R.G., and Hancock, J.F. (2008). Activation of the MAPK module from different spatial locations generates distinct system outputs. Mol. Biol. Cell *19*, 4776–4784.

Johnson, D.S., and Chen, Y.H. (2012). Ras family of small GTPases in immunity and inflammation. Curr. Opin. Pharmacol. *12*, 458–463.

Jung, K., Dihazi, H., Bibi, A., Dihazi, G.H., and Beißbarth, T. (2014). Adaption of the global test idea to proteomics data with missing values. Bioinformatics *30*, 1424–1430.

Jura, N., Scotto-Lavino, E., Sobczyk, A., and Bar-Sagi, D. (2006). Differential modification of Ras proteins by ubiquitination. Mol. Cell *21*, 679–687.

Karnoub, A.E., and Weinberg, R.A. (2008). Ras oncogenes: split personalities. Nat. Rev. Mol. Cell Biol. *9*, 517–531.

Karpievitch, Y.V., Dabney, A.R., and Smith, R.D. (2012). Normalization and missing value imputation for label-free LC-MS analysis. BMC Bioinformatics *13* (*Suppl 16*), S5.

Keshava Prasad, T.S., Goel, R., Kandasamy, K., Keerthikumar, S., Kumar, S., Mathivanan, S., Telikicherla, D., Raju, R., Shafreen, B., Venugopal, A., et al. (2009). Human Protein Reference Database–2009 update. Nucleic Acids Res. *37*, D767–D772.

Koseoglu, M.M., Ozdilek, B.A., Djakbarova, U., and Gulusur, A. (2016). Targeting Ras Activity Prevented Amyloid Beta-Induced Aberrant Neuronal Cell Cycle Re-Entry and Death. Curr. Alzheimer Res. *13*, 1267–1276.

Kruiswijk, F., Labuschagne, C.F., and Vousden, K.H. (2015). p53 in survival, death and metabolic health: a lifeguard with a licence to kill. Nat. Rev. Mol. Cell Biol. *16*, 393–405.

Linding, R., Jensen, L.J., Ostheimer, G.J., van Vugt, M.A., Jorgensen, C., Miron, I.M., Diella, F., Colwill, K., Taylor, L., Elder, K., et al. (2007). Systematic discovery of *in vivo* phosphorylation networks. Cell *129*, 1415–1426.

Liu, R., Liu, D., and Xing, M. (2012). The Akt inhibitor MK2206 synergizes, but perifosine antagonizes, the BRAF(V600E) inhibitor PLX4032 and the MEK1/2 inhibitor AZD6244 in the inhibition of thyroid cancer cells. J. Clin. Endocrinol. Metab. *97*, E173–E182.

Lorentzen, A., Kinkhabwala, A., Rocks, O., Vartak, N., and Bastiaens, P.I. (2010). Regulation of Ras localization by acylation enables a mode of intracellular signal propagation. Sci. Signal. *3*, ra68.

Matallanas, D., Sanz-Moreno, V., Arozarena, I., Calvo, F., Agudo-Ibáñez, L., Santos, E., Berciano, M.T., and Crespo, P. (2006). Distinct utilization of effectors and biological outcomes resulting from site-specific Ras activation: Ras functions in lipid rafts and Golgi complex are dispensable for proliferation and transformation. Mol. Cell. Biol. *26*, 100–116.

Million, R.P., and Van Etten, R.A. (2000). The Grb2 binding site is required for the induction of chronic myeloid leukemia-like disease in mice by the Bcr/Abl tyrosine kinase. Blood *96*, 664–670.

Mor, A., Campi, G., Du, G., Zheng, Y., Foster, D.A., Dustin, M.L., and Philips, M.R. (2007). The lymphocyte function-associated antigen-1 receptor costimulates plasma membrane Ras via phospholipase D2. Nat. Cell Biol. *9*, 713–719.

Munoz, J., Dhillon, N., Janku, F., Watowich, S.S., and Hong, D.S. (2014). STAT3 inhibitors: finding a home in lymphoma and leukemia. Oncologist *19*, 536–544.

O'Neill, E., Rushworth, L., Baccarini, M., and Kolch, W. (2004). Role of the kinase MST2 in suppression of apoptosis by the proto-oncogene product Raf-1. Science *306*, 2267–2270.

Oba, D., Inoue, S.I., Miyagawa-Tomita, S., Nakashima, Y., Niihori, T., Yamaguchi, S., Matsubara, Y., and Aoki, Y. (2018). Mice with an Oncogenic HRAS Mutation are Resistant to High-Fat Diet-Induced Obesity and Exhibit Impaired Hepatic Energy Homeostasis. EBioMedicine *27*, 138–150.

Perez-Riverol, Y., Csordas, A., Bai, J., Bernal-Llinares, M., Hewapathirana, S., Kundu, D.J., Inuganti, A., Griss, J., Mayer, G., Eisenacher, M., et al. (2019). The PRIDE database and related tools and resources in 2019: improving support for quantification data. Nucleic Acids Res. *47* (*D1*), D442–D450.

Procaccia, S., Ordan, M., Cohen, I., Bendetz-Nezer, S., and Seger, R. (2017). Direct binding of MEK1 and MEK2 to AKT induces Foxo1 phosphorylation, cellular migration and metastasis. Sci. Rep. *7*, 43078.

Pylayeva-Gupta, Y., Grabocka, E., and Bar-Sagi, D. (2011). RAS oncogenes: weaving a tumorigenic web. Nat. Rev. Cancer *11*, 761–774.

Ramdzan, Z.M., and Nepveu, A. (2014). CUX1, a haploinsufficient tumour suppressor gene overexpressed in advanced cancers. Nat. Rev. Cancer *14*, 673–682.

Ramdzan, Z.M., Vadnais, C., Pal, R., Vandal, G., Cadieux, C., Leduy, L., Davoudi, S., Hulea, L., Yao, L., Karnezis, A.N., et al. (2014). RAS transformation

requires CUX1-dependent repair of oxidative DNA damage. PLoS Biol. *12*, e1001807.

Rocks, O., Peyker, A., Kahms, M., Verveer, P.J., Koerner, C., Lumbierres, M., Kuhlmann, J., Waldmann, H., Wittinghofer, A., and Bastiaens, P.I. (2005). An acylation cycle regulates localization and activity of palmitoylated Ras isoforms. Science *307*, 1746–1752.

Rohart, F., Gautier, B., Singh, A., and Lê Cao, K.A. (2017). mixOmics: An R package for 'omics feature selection and multiple data integration. PLoS Comput. Biol. *13*, e1005752.

Rose, D.W., Xiao, S., Pillay, T.S., Kolch, W., and Olefsky, J.M. (1998). Prolonged vs transient roles for early cell cycle signaling components. Oncogene *17*, 889–899.

Rubin, S.M. (2013). Deciphering the retinoblastoma protein phosphorylation code. Trends Biochem. Sci. *38*, 12–19.

Santra, T. (2016). A Bayesian non-parametric method for clustering high-dimensional binary data. arXiv, arXiv:160302494. https://arxiv.org/abs/1603.02494.

Santra, T., Kolch, W., and Kholodenko, B.N. (2013). Integrating Bayesian variable selection with Modular Response Analysis to infer biochemical network topology. BMC Syst. Biol. *7*, 57.

Singh, R., Park, D., Xu, J., Hosur, R., and Berger, B. (2010). Struct2Net: a web service to predict protein-protein interactions using a structure-based approach. Nucleic Acids Res. *38*, W508–W515.

Song, C., Ye, M., Liu, Z., Cheng, H., Jiang, X., Han, G., Songyang, Z., Tan, Y., Wang, H., Ren, J., et al. (2012). Systematic analysis of protein phosphorylation networks from phosphoproteomic data. Mol. Cell. Proteomics *11*, 1070–1083.

Stingele, S., Stoehr, G., Peplowska, K., Cox, J., Mann, M., and Storchova, Z. (2012). Global analysis of genome, transcriptome and proteome reveals the response to aneuploidy in human cells. Mol. Syst. Biol. *8*, 608.

Sun, Y., Cheng, Z., Ma, L., and Pei, G. (2002). Beta-arrestin2 is critically involved in CXCR4-mediated chemotaxis, and this is mediated by its enhancement of p38 MAPK activation. J. Biol. Chem. *277*, 49212–49219.

Swaney, D.L., McAlister, G.C., and Coon, J.J. (2008). Decision tree-driven tandem mass spectrometry for shotgun proteomics. Nat. Methods *5*, 959–964.

Szklarczyk, D., Franceschini, A., Wyder, S., Forslund, K., Heller, D., Huerta-Cepas, J., Simonovic, M., Roth, A., Santos, A., Tsafou, K.P., et al. (2015). STRING v10: protein-protein interaction networks, integrated over the tree of life. Nucleic Acids Res. *43*, D447–D452.

Thorsson, V., Gibbs, D.L., Brown, S.D., Wolf, D., Bortone, D.S., Ou Yang, T.H., Porta-Pardo, E., Gao, G.F., Plaisier, C.L., Eddy, J.A., et al.; Cancer Genome Atlas Research Network (2018). The Immune Landscape of Cancer. Immunity *48*, 812–830.e14.

Turriziani, B., Garcia-Munoz, A., Pilkington, R., Raso, C., Kolch, W., and von Kriegsheim, A. (2014). On-beads digestion in conjunction with data-dependent mass spectrometry: a shortcut to quantitative and dynamic interaction proteomics. Biology (Basel) *3*, 320–332.

Welburn, J.P., Tucker, J.A., Johnson, T., Lindert, L., Morgan, M., Willis, A., Noble, M.E., and Endicott, J.A. (2007). How tyrosine 15 phosphorylation inhibits the activity of cyclin-dependent kinase 2-cyclin A. J. Biol. Chem. *282*, 3173–3181.

Wu, Y., Williams, E.G., Dubuis, S., Mottis, A., Jovaisaite, V., Houten, S.M., Argmann, C.A., Faridi, P., Wolski, W., Kutalik, Z., et al. (2014). Multilayered genetic and omics dissection of mitochondrial activity in a mouse reference population. Cell *158*, 1415–1430.

Yang, J.S., Campagna, A., Delgado, J., Vanhee, P., Serrano, L., and Kiel, C. (2012). SAPIN: a framework for the structural analysis of protein interaction networks. Bioinformatics *28*, 2998–2999.

Zagórska, A., Deak, M., Campbell, D.G., Banerjee, S., Hirano, M., Aizawa, S., Prescott, A.R., and Alessi, D.R. (2010). New roles for the LKB1-NUAK pathway in controlling myosin phosphatase complexes and cell adhesion. Sci. Signal. *3*, ra25.

Zhang, B., Wang, J., Wang, X., Zhu, J., Liu, Q., Shi, Z., Chambers, M.C., Zimmerman, L.J., Shaddox, K.F., Kim, S., et al.; NCI CPTAC (2014). Proteogenomic characterization of human colon and rectal cancer. Nature *513*, 382–387.

Zhong, J. (2016). RAS and downstream RAF-MEK and PI3K-AKT signaling in neuronal development, function and dysfunction. Biol. Chem. *397*, 215–222.

Zhou, H., Ye, M., Dong, J., Corradini, E., Cristobal, A., Heck, A.J., Zou, H., and Mohammed, S. (2013). Robust phosphoproteome enrichment using monodisperse microsphere-based immobilized titanium (IV) ion affinity chromatography. Nat. Protoc. *8*, 461–480.

STAR★METHODS

KEY RESOURCES TABLE

REAGENT or RESOURCE	SOURCE	IDENTIFIER
Antibodies		
anti-Flag M2 Agarose	Sigma-Aldrich	A-2220; RRID: AB_10063035
anti-Flag M2-Peroxidase	Sigma-Aldrich	A8592; RRID: AB_439702
anti-p53 DO-1	Santa Cruz	SC-126; RRID: AB_628082
anti-Tubulin TU-02	Santa Cruz	SC-8035; RRID: AB_628408
anti-PDCD2	Abcam	AB133324; RRID: AB_11158526
anti-GAPDH	Abcam	AB9485; RRID: AB_307275
anti-phospho (P)-MAPK/CDK substrate	Cell Signaling Technologies	2325S; RRID: AB_331820
anti-cJUN (60A8)]	Cell Signaling Technologies	9165S; RRID: AB_2130165
anti-EGFR	Cell Signaling Technologies	3265S; RRID: AB_2262057
anti-BRAF	Santa Cruz	Sc-5284; RRID: AB_626760
anti-SOS1	Santa Cruz	Sc-376789; RRID: not available
Chemicals, Peptides, and Recombinant Proteins		
MEK inhibitor U0126	Promega	V112A
p38 inhibitor SB203580	Calbiochem	CAS 152121-47-6
Lipofectamine	ThermoFisher	11668019
G418	ThermoFisher	10131027
Phosphatase Inhibitor Cocktail Set III	Sigma Aldrich	524627
Protease Inhibitor Cocktail	Roche	11 836 153 001
Critical Commercial Assays		
Vybrant Apoptosis Assay Kit #4	ThermoFisher	V13243
Oris Cell Migration Assay	Platypus	CMA1.101
Deposited Data		
Gene array expression data	ArrayExpress	E-MTAB-7672
HRASV12 interaction proteomics data	ProteomeXchange	PXD012505
Phosphoproteomics data	ProteomeXchange	PXD012506
Experimental Models: Cell Lines		
HeLa cell lines expressing pCEFL-Flag-HRASV12 targeted constructs	This study	N/A
HeLa cell lines expressing pCEFL-Flag-HRASV12 targeted constructs	Herrero et al., 2018; Matallanas et al., 2006	N/A
Oligonucleotides		
Untargeted control siRNA	Dharmacon	D-001810-01-20
siRNA targeting p53	Dharmacon	J-003329-17
siRNA targeting PDCD2	Dharmacon	L-004437-00-005
Recombinant DNA		
pCEFL-Flag-HRASV12 targeted constructs	Herrero et al., 2018; Matallanas et al., 2006	N/A
pCEFL-Flag-CDC25 targeted constructs	Herrero et al., 2018; Matallanas et al., 2006	N/A
Software and Algorithms		
MATLAB v6	Mathworks	https://uk.mathworks.com/

CONTACT FOR REAGENT AND RESOURCE SHARING

Further information and requests for resources and reagents should be directed to and will be fulfilled by the Lead Contact, David Matallanas-Gomez (david.gomez@ucd.ie).

EXPERIMENTAL MODEL AND SUBJECT DETAILS

HeLa cells were grown in Dulbecco's modified medium (DMEM) supplemented with 10% fetal bovine serum (FBS). Sub-confluent HeLa cell lines were transfected with 1μg of HRASV12 or CDC25 expression vectors (carrying a G418 resistance gene) using Lipofectamine (GIBCO) following the manufacturer's instructions. 24 hours after transfection cells were selected by adding 400μg/ml of G418 until macroscopically visible colonies formed. Subsequently, the colonies were trypsinized, pooled and expanded. The expression of exogenous proteins was verified by immunoblotting with Flag antibody. The cells used in the experiments were grown in the absence of G418 to avoid potentially confounding effects from G418. However, cell stocks were put into selection media every 4 passages and the expression of exogenous proteins was regularly monitored to confirm proper expression of the constructs. Flag-HRASV12 targeted constructs and pCEFL-Flag-CDC25 targeted constructs are cloned in pCEFL and were described before (Herrero et al., 2018; Matallanas et al., 2006).

METHOD DETAILS

Experimental Methods

Cell lysates and immunoblots

Cells were lysed in ice cold cell lysis buffer containing 20mM HEPES pH 7.5, 150mM NaCl, 1% NP-40, protease inhibitors (1μM leupeptin and aprotinin; Sigma) and phosphatase inhibitors (10mM β-Gycerolphosphate, 2 mM $Na_4P_2O_4$; Roche). Control, TP53 and PDCD2 (60pM) siRNAs were transfected using Lipofectamine and cells were lysed 48 hours after transfection. Total lysates were resolved by SDS-polyacrylamide gel electrophoresis and transferred to a PVDF membrane.

Migration assay

HeLa cell lines stably expressing CDC25 constructs were examined for migration using the Oris Cell Migration Assay. Cells were seeded in a 96-well plate (30,000cells/well) containing the ''Oris cell seeding stoppers'' which exclude cells from a central circular area. After 24 hours stoppers were removed, and cells were cultivated in growing media (10% FBS) for 24 hours to permit cells to migrate into the void area. For inhibition assays 5μM U0126 MEK inhibitor or 10μM SB203580 p38 inhibitor were added when the stoppers were removed. Prior to analysis cells were stained with calcein for 30 minutes and pictures were taken. Cellular migration was quantified using ImageJ by measuring the percentage of the void area covered.

Apoptosis was measured in cells that had been serum starved for 32 hours. Two types of apoptosis assays were used. One measured DNA fragmentation, which is a late marker of apoptosis. This assay uses propidium iodide staining and quantitation of the sub-G1 peak representing fragmented DNA using flow cytometry as previously described (O'Neill et al., 2004). The other assay used the Vybrant Apoptosis Assay Kit #4 (Thermo Fisher) according to the manufacturer's instructions. This assay detects changes in the membrane permeability of apoptotic cells in the early phase of apoptosis. Assays were performed three times.

Proliferation assays

HeLa stable cell lines expressing CDC25 at different subcellular localizations were seeded in 6 wells plates (25.000 cells/well), and transfected with 60pmol of p53 siRNA. Proliferation was monitored in two independent experiments by counting cells after growing them for 48 hours in full medium containing 5% FBS.

Interaction proteomics experiments were done as previously described (Turriziani et al., 2014). Briefly, HeLa cell lines stably expressing HRASV12 or targeted derivative constructs were serum starved for 16 hours to reach a steady state of HRASV12 signaling that is not confounded by serum growth factor effects. Cells were lysed in ice cold lysis buffer (1% NP40, 20mM Tris-HCl pH 7.5, 150mM NaCl, 1mM $MgCl_2$) containing protease inhibitor cocktail (Roche) and phosphatase inhibitors (2mM sodium orthovanadate, 10mM sodium fluoride and 10mM β-glycerophosphate; Sigma-Aldrich). Lysates were cleared from debris by centrifugation at 4°C and 18,000xg for 10 minutes, and total protein concentration of the supernatants was determined by the Pierce BCA assay (Thermo Fisher). Lysates were adjusted to equal protein concentrations and incubated with 10 μL of Flag-M2 agarose beads (Sigma-Aldrich) for 2 hours at 4°C. The beads were washed twice with lysis buffer, and trice with TBS (10mM Tris-HCl pH 7.4, 150mM NaCl) to remove detergent. Then, the Flag-HRASV12 immunoprecipitates were digested with trypsin, reduced, and alkylated exactly as described previously (Turriziani et al., 2014). Tryptic peptides were analyzed on a Thermo Scientific Q-Exactive MS connected to an Ultimate Ultra3000 chromatography system incorporating an autosampler. Data were acquired with the MS operating in automatic data-dependent switching mode, selecting the 12 most intense ions prior to tandem MS analysis. MS raw data were analyzed by the MaxQuant software (Cox and Mann, 2008). Specifically, tandem MS spectra were searched against the human Uniprot database with a mass accuracy of 4.5 ppm and 20 ppm (for MS and MS/MS). Carbamylation was selected as fixed modification. Variable modifications were N-terminal acetylation (protein) and oxidation (M). FDR was set to 0.01. LFQ and peak matching was selected and was limited to within a 30 s elution window with a mass accuracy of 4.5 ppm. The results are based on 3 independent biological replicates.

Phosphoproteomics experiments

HeLa cell lines stably expressing empty vectors, Flag-CDC25 or targeted derivative constructs (Herrero et al., 2018) were serum starved for 16 hours, washed with PBS and then snap frozen at −70°C. Frozen cells were lysed on ice by sonication in phospho-lysis buffer (50mM ammonium bicarbonate, pH 8.0; 8 M urea; 1mM sodium orthovanadate, Sigma-Aldrich; complete EDTA-free protease inhibitors, Roche; and phosSTOP phosphatase inhibitors, Roche). Cell debris was removed by centrifugation at 20,000 × g for 15 minutes at 4°C. The total protein concentration was estimated using a Bradford Assay (BioRad). Then, 1mg of total protein was reduced with 1mM dithiothreitol (DTT, Sigma-Aldrich) and alkylated with 5.5mM iodoacetamide (IAA, Sigma-Aldrich). Proteolytic digestion of proteins were subsequently performed at 37°C, first with endoproteinase Lys-C (Wako Chemicals) for 4 hours, followed by sequencing-grade modified trypsin (Promega) overnight, after 4-fold dilution of phospho-lysis buffer with 50mM ammonium bicarbonate. Proteolysis was stopped by the addition of trifluoroacetic acid (TFA, Sigma-Aldrich) to a final concentration of 1%. Tryptic peptides were desalted using Sep-Pak C18 cartridges (Waters) and dried in vacuo.

Enrichment of phosphopeptides with Ti^{4+}-IMAC was performed as previously described (Zhou et al., 2013). Briefly, each Ti^{4+}-IMAC column was constructed by loading Ti^{4+}-IMAC beads (500 μg of beads/200 μL pipette tip) into a GELoader tip (Eppendorf, Hamburg, Germany) blocked with a plug made of Empore C8 material (3M) at the tapered end. Each Ti^{4+}-IMAC column was then conditioned with 50 μL of loading buffer (6% TFA in 80% acetonitrile, ACN) prior to use. Protein digests were dissolved in 80% ACN/6% TFA and split in aliquots of 200μg each, sufficient for technical triplicates per biological sample. Each column was loaded with 200 μg of peptide digest and centrifuged at 100 × g for 30 min. They were then sequentially washed with 50 μL of washing buffer 1 (50% ACN, 0.5% TFA containing 200mM NaCl) followed by additional washing with 50 μL of 0.1% TFA in 50% ACN, each time centrifuged at 170 × g for 15 min. Bound peptides were eluted with 20 μL of 10% ammonia by centrifugation at 100 × g for 20 min into a new tube containing 35 μL of 10% formic acid (FA). A final elution was performed with 5 μL of 2% FA in 80% ACN at 100 × g for 10 min. The pooled eluate was acidified by adding 3 μL of 100% FA.

nanoLC-MS/MS Analysis was performed by separating peptides using a Proxeon EASY-nLC 1000 (Thermo Scientific) with an analytical column heater (40°C) and a C18 reversed phase column connected to a LTQ-Orbitrap Elite (Thermo Scientific). Injected peptides were first trapped (Dr Maisch Reprosil C18, 3 μm, 2cm x 100 μm) at a maximum pressure of 800 bar with 100% solvent A (0.1% FA in water) before being separated on the analytical column (Agilent Poroshell 120 EC-C18, 2.7 μm, 40cm x 50 μm) using a 120 minute gradient at a flow rate of 100nL/min as follows: (i.) 7% to 30% solvent B (91min); (ii.) 30% to 100% solvent B (3min); (iii.) 100% to 100% solvent B (5min); (iv.) 100% to 7% solvent B (1min) and (v.) 7% to 7% solvent B (20min). The eluent was sprayed via a distal coated fused silica emitter (360 μm o.d., 20 μm i.d., 10 μm tip i.d.; constructed in-house). The electrospray voltage was set to 1.7kV. The mass spectrometer was operated in a data-dependent mode to automatically switch between MS and MS/MS. Briefly, survey full-scan MS spectra were acquired in the Orbitrap analyzer, scanning from m/z 350 to m/z 1500 at a resolution of 60,000 at m/z 400 using an AGC setting of 1e6 ions. Charge state screening was enabled, and precursors with either unknown or 1+ charge states were excluded. After the survey scan the 20 most intense precursors were selected for subsequent decision tree-based ion trap CID or ETD fragmentation (Frese et al., 2011; Swaney et al., 2008). The normalized collision energy for CID was set to 35% and supplemental activation for ETD and dynamic exclusion were enabled (exclusion size list 500, exclusion duration 60 s). Experiments were performed in 3 biological and 2 technical replicates for each of the 6 cell lines.

nanoLC-MS/MS Data Processing

Raw data files from 36 experiments (3 biological and 2 technical replicates for each of 6 experimental conditions) were processed with MaxQuant version 1.3.0.5 (Cox and Mann, 2008). MS and MS/MS spectra were searched against concatenated forward-decoy SwissProt *Homo sapiens* database (2013/07; 40,992 sequences) using the Andromeda search engine. The database search was performed with the following parameters: an initial mass tolerance of ± 20 ppm and a final mass tolerance of ± 6 ppm for precursor masses, ± 0.6 Da for CID and ETD ion trap fragment ions, with two missed cleavages allowed. Cysteine carbamidomethylation was used as a fixed modification, and methionine oxidation, protein N-terminal acetylation, and serine, threonine, and tyrosine phosphorylation were included as variable modifications. The false discovery rate was set at 0.01 for peptides, proteins, and phosphosites; the minimum peptide length allowed was six amino acids; and a minimum Andromeda peptide score of 60 was required. The match-between-runs feature was enabled. A site localization probability of at least 0.75 and a score difference of at least 5 were used as thresholds for the localization of phospho-residues. Normalization was performed by subtracting the median of log transformed intensities for each nanoLC-MS/MS run. To identify significantly regulated phosphorylation sites, a two-sample t test was performed with a permutation-based false discovery rate of 0.005 (randomizations were set at 500, and s0 was tuned to achieve a minimum 2-fold regulation and varied between 0.35 and 0.4).

Transcriptomics experiments

Triplicates of HeLa cell lines stably expressing empty vector (pCEFL), HRASV12 or targeted derivative constructs were serum starved for 16 hours. Then, RNA was extracted using the RNAsy method following manufacturer's (Quiagen) recommendations and analyzed on the Affymetrix GeneChip® Scanner 3000 7G System using chip MGU75v2 according to the manufacturer's protocol. Three independent experiments were performed.

DATA ANALYSIS AND COMPUTATIONAL MODELS

Interactome analysis pipeline

Missing values in the MS data were imputed as follows: Protein intensities were log-transformed and the logarithmic intensities of a protein measured in a certain experimental condition were assumed to have normal distribution (Jung et al., 2014; Karpievitch et al., 2012). If a certain experiment was replicated N times and a protein P was observed in M ($1 < M < N$) replicates but was missing from the remaining (N-M) replicates, then the missing values were replaced by random numbers which were sampled from a normal distribution with mean and variance equal to the sample mean and variance of the observed intensities. When a protein was observed in only one replicate ($M = 1$) in a certain experimental condition, the missing intensities were replaced by the observed intensity. In all other cases, i.e., when protein intensities were missing from all replicates, intensities were replaced by zero. The imputed data was used to find differential HRASV12 interactors. We used a combination of fold change and t test followed by Benjamini Hochberg False Discovery Rate (FDR) correction for this purpose. The optimal FDR threshold was selected by maximizing the ratio of the number of known RAS interactors that pass the test versus the total number of potential interactors. The fold change threshold was set to 1.5. Among the potential interactors selected by the above pipeline, the ones that were found to interact with RAS in the STRING (Szklarczyk et al., 2015) or HPRD (Keshava Prasad et al., 2009) databases and were predicted to interact with RAS by Struct2Net (Singh et al., 2010) or SAPIN (Yang et al., 2012) were assumed to be the most likely direct RAS interactors. The ones which were supported by one of the above data sources were assumed to be the next most likely interactors. The remaining proteins were assumed to be either novel or indirect interactors of RAS. For Figure 1B proteins were clustered according to their GO terms (Santra, 2016), and the resulting clusters were labeled by the GO term common to most proteins in the cluster.

Phosphoproteomics data analysis pipeline

Missing values in the MS data was imputed as described in the interaction proteomics section above. Differentially phosphorylated peptides were identified using a combination of fold-change, t test and Benjamini Hochberg FDR correction. In this case the fold change and FDR threshold were set to 1.5 and 0.05, respectively. Only those phosphopeptides which were highly phosphorylated in samples where HRAS was activated at different locations compared to control were selected for kinase- substrate (K-S) network reconstruction analysis.

First, as training dataset we analyzed experimentally validated K-S pairs obtained from the PhosphoELM and PhosphositePlus databases, and calculated two position weight matrices (PWM) for each kinase (k). One PWM represents the distribution of amino-acids (AAs) in the neighborhood of the phosphorylation sites that are targeted by k, and the other PWM represents the same for the phosphorylation sites that are not targeted by k. Each PWM is a $20 \times N_w$ matrix whose rows represent the 20 natural amino acids (AAs) that occur in proteins, and the columns represent the positions across a sequence window of length N_w centered around a certain phosphosite. An element P_{ij} of this matrix represent the probability of the i^{th} AA to appear at the j^{th} position in the sequence window. The PWMs were calculated in the following manner. For each kinase (k), we assembled two ensembles of small ($N_w = 15$) peptides from the above databases. The first ensemble contains the peptides which were found to be phosphorylated by kinase k at their central position (8th AA), and the second ensemble contains the peptides which were not phosphorylated by kinase k. For notational convenience, we refer the first and second ensembles as positive (D^{k+}) and negative (D^{k-}) datasets of kinase k, respectively. These two datasets (D^{k+} & D^{k-}) were then used to calculate the positive ($\boldsymbol{P}^{\boldsymbol{k}+}$) and negative ($\boldsymbol{P}^{\boldsymbol{k}-}$) position weight matrices (PWMs) of kinase k. The elements (P_{ij}^{k+}) of the positive PWM (P_{ij}^{k+}) represent the probability that the i^{th} AA (out of 20 possible AAs) occur at the j^{th} ($j = 1, ..7, 9..15$) position in the peptides that belong to the positive dataset (D^{k+}) of kinase k. This probability (P_{ij}^{k+}) was estimated by $\frac{N_{ij}+0.05}{N+1}$ where N_{ij} is number of times the i^{th} amino acid occurs at the j^{th} site, and N is the total number of peptides in the positive dataset. Similarly, the elements (P_{ij}^{k-}) of $\boldsymbol{P}^{\boldsymbol{k}-}$ represent the probability that the i^{th} AA occur at the j^{th} position in the phosphopeptides which belong to the negative dataset (D^{k-}) of kinases k. These probabilities (P_{ij}^{k-}) were estimated using the negative dataset ac (D^{k-}) in a similar manner as P_{ij}^{k+}. The positive and negative PWMs ($\boldsymbol{P}^{\boldsymbol{k}+}$ & $\boldsymbol{P}^{\boldsymbol{k}-}$) of each kinase k were used to determine its potential targets among the phosphopeptides that were found to be significantly phosphorylated in our MS data. To determine whether a phosphopeptide p is phosphorylated by a kinase k, we calculated the probabilities that its sequence has the same distribution as the peptides in the positive (D^{k+}) or negative (D^{k-}) datasets of kinase k. These probabilities, also known as likelihoods, are denoted by ϕ_{pk}^{+} and ϕ_{pk}^{-}, respectively, and are calculated as $\phi_{pk}^{+} = \prod_{i=1\,j=1\,j\neq 8}^{i=20\,j=15} P_{ij}^{k+} I_{ij}$ and $\phi_{pk}^{-} = \prod_{i=1\,j=1\,j\neq 8}^{i=20\,j=15} P_{ij}^{k-} I_{ij}$, where $I_{ij} = 1$ if the i^{th} amino acid occurs at the j^{th} position of the phosphopeptide p, and $I_{ij} = 0$ otherwise. In theory, $\phi_{pk}^{+} > \phi_{pk}^{-}$ indicates that kinase k potentially phosphorylates phosphopeptide p. However, to ensure that the difference between ϕ_{pk}^{+} & ϕ_{pk}^{-} is statistically significant, these two entities were compared using a likelihood-ratio test which produces a p value that indicates the level of statistical significance, with smaller p values being indicative of higher significance. These tests were performed for each kinase in the training dataset versus each significantly phosphorylated phosphopeptide in the MS data. The resulting p values were then used to estimate the FDR using the Benjamini Hochberg method. Interactions with FDR < 0.05 were selected as potential K-S interaction. The above analysis resulted in four K-S interaction networks (phosphorylation networks), one for each subcellular localization of RAS.

The above phosphorylation networks are likely to contain false K-S interactions due to the following reasons. In most cases, kinases belonging to the same kinase-group recognize highly similar consensus sequence motifs. Consequently, if a phosphopeptide contains a certain motif that is recognized by a certain kinase, it is highly likely that the motif is also recognized by other kinases in the same group. To add further specificity to the inferred K-S interactions, we included the criterion that kinase and substrate have to physically interact. For this we employed the STRING (Szklarczyk et al., 2015) and HPRD (Keshava Prasad et al., 2009) protein-protein interaction (PPI) databases, and retained all K-S interactions which were supported by existing PPI interactions, while excluding the remaining interactions from further analysis (Song et al., 2012).

Accuracy Assessment of the Kinase-Substrate Prediction was performed by benchmarking the predictions of our algorithm against (i) PhosphositePlus, which is a highly curated database that collects experimental information on phosphorylation sites, their function and the kinases responsible by human literature studies (https://www.phosphosite.org/homeAction.action); and (ii) NetworKIN (http://networkin.info/), which is a widely used tool for the prediction of kinase-substrate pairs that is backed by high profile publications (Horn et al., 2014; Linding et al., 2007). Focusing on the peptides that are shared between our dataset and the PhosphositePlus dataset, we calculated the accuracy and the precision for each kinase. The accuracy is the number of peptides correctly predicted to be phosphorylated by the kinase (true positives) added to the number of peptides correctly predicted not to be phosphorylated by the kinase (true negatives) and dividing this sum by the total number of peptides. Similarly, the precision is defined as the number of true positives divided by the total number of peptides predicted by our algorithm to be phosphorylated by the kinase. Finally, we repeated the same procedure with the NetworKIN algorithm (Linding et al., 2007) and compared the results with the accuracy and precision of our algorithm. The results show that the accuracy of our method is very high (~98%). Comparing our method to NetworKIN predictions, our algorithm has a better or similar accuracy for 20 kinases out of 54 tested for which this algorithm can make predictions. These data are included in Figure S2B and Table S2.

Transcriptomic data analysis pipeline

We first excluded the low variance (lowest 10^{th} percentile) genes using MATLAB's variance filter. Then we used one-way-ANOVA to identify genes whose expression is influenced by HRAS localizations. The p values produced by ANOVA were further corrected using Benjamini Hochberg's FDR method. Genes with FDR < 0.05 were then selected for further analysis.

The selected genes were used for differential expression analysis, clustering and transcriptional regulatory network (TRN) reconstruction. We used t test followed by Benjamini-Hochberg's FDR correction to identify genes which were differentially expressed between control samples and samples where HRASV12 signaled from different subcellular locations. Clustering was performed using MATLAB's 'clustergram' tool.

For TRN reconstruction, we first developed a prior network model of transcription regulations between TFs and genes which were selected by the ANOVA analysis. This was done by combining existing ChIPseq data from the ENCODE database, PPI data from the STRING (Szklarczyk et al., 2015) and HPRD (Keshava Prasad et al., 2009) databases, and gene ontology data from the Gene Ontology Consortium (http://geneontology.org/). While the ChIPseq data was used to determine direct TF-DNA interactions, PPIs between TFs were used to identify transcriptional regulators which do not bind to genes directly, but regulate genes by binding to cognate TFs. GO annotations were used to find TFs and genes with shared functionalities. This was done by clustering the filtered genes according to their GO terms using the BNPBDCA algorithm (Santra, 2016). TFs and genes sharing the same cluster were assumed to belong to the same functional categories and therefore are likely to interact to each other. The transcriptional interactions which were

(a) supported by all three types of information were assigned the highest score of 1.
(b) supported by ChIPseq data and at least one of PPI and GO data were assigned the second highest score of 0.8.
(c) supported by PPI and GO data, but not ChIP-seq data were assigned the third highest score (0.6)
(d) supported by only PPI data were assigned the fourth highest score of 0.4.
(e) supported by only GO data were assigned the smallest score of 0.2.
(f) not supported by any of the above data were assigned a score of 0.

The weighted prior gene regulation model ($\boldsymbol{A}_i^{prior}$) of each gene (i) was then used to formulate the prior distribution of its transcriptional model ($\boldsymbol{A}_i$) using the following formula: $P(\boldsymbol{A}_i) = \exp(-\mathbf{A}_i^{T}\mathbf{A}_i^{\text{prior}} + \mathrm{A}_i^{\mathrm{T}}\mathbf{B}_i\mathrm{A}_i)$ (Higdon, 1998). Here, $\boldsymbol{A}_i^{prior}$ is a $N_{TF} \times 1$ vectors whose j^{th} element contains the prior interaction score between the j^{th} TF and the i^{th} gene. $\boldsymbol{A}_i$ is a $N_{TF} \times 1$ binary vector whose j^{th} element is 1 if the j^{th} TF regulates the i^{th} gene and 0 otherwise, N_{TF} is the number of TFs. $\boldsymbol{B_i}$ is a $N_{TF} \times N_{TF}$ matrix whose element B_i^{jk} in the j^{th} row and k^{th} column has a constant value $\beta = 0.01$ if the j^{th} and k^{th} TFs bind to each other and 0 otherwise. Inclusion of the PPIs between TFs makes it likely that TFs that belong to the same TF complex are selected as co-regulators of the same set of genes. The prior distribution was used in a Bayesian Variable Selection (BVS) framework as described in (Santra et al., 2013). The BVS algorithm updated the prior gene regulation model ($\boldsymbol{A}_i^{prior}$) using the transcriptomic data, produced in our experiments, and yielded posterior models of gene regulations ($\boldsymbol{A}_i^{posterior}$) (Santra et al., 2013). The posterior gene regulation model ($\boldsymbol{A}_i^{posterior}$) is represented by a $N_{TF} \times 1$ binary vector whose j^{th} element contains the probability (termed interaction probability in Figure 3F) that the i^{th} gene is regulated by the j^{th} TF in the context of our experiment. The sum of all interaction probabilities (rounded to the closest integer) involving each gene set influenced by HRASV12 from different subcellular locations is termed the expected number of interactions. As detailed above, interaction

probability is a score calculated from ChIP data, PPIs between TFs and, shared GO terms between TF-gene pairs and gene expressions, which designates the probability that a TF regulates a gene on a scale of 0 to 1.

Expected in- and out-degrees *(Figure 3F)*

The average expected in-degrees indicate how many TFs regulate a gene based on the sum of all incoming interaction probabilities for each gene averaged over the number of genes. Similarly, the average expected out-degrees describing how many genes are regulated by a TF based on the sum of all outgoing interaction probabilities of each TF averaged over all TFs regulating a gene set.

Pathway enrichment analyses were performed using DAVID version 6.8 (Huang et al., 2009a, 2009b). DAVID allows various pathway definitions for this type of analysis. We used KEGG pathway definitions and default parameter settings for the analysis.

Gene Ontology (GO) enrichment analyses were performed using PANTHER which is the default GO enrichment analysis tool in http://geneontology.org/. We used default parameter settings for these analyses.

Calculation of pathway signaling capacities (Figure S3B) was done by counting the total number of interactions involving the components of each pathway in the integrated multilayer interactomes.

Development of MiNETi

MiNETi is a conceptual framework for creating multi-layer biochemical networks. It is based on the principle that data displayed as a network allow us to connect nodes between networks by logical or empirical rules. These rules can be added or deleted as knowledge evolves, and their importance can be statistically weighted, resulting in a flexible, updatable framework that can in principle be used to integrate any type of data that can be visualized as network and where nodes are connectable via their properties. Here, to demonstrate the principle we have used MiNETi to analyze interaction proteomic, phosphoproteomic and transcriptomic data. Below we describe the assumptions and rules we used to combine the three networks.

Step 1

The CoIP-MS screens followed by statistical analysis revealed proteins which appear with significantly higher intensities in HRASV12 expressing cells than in empty vector control cells (Table S1). However, the CoIP screens do not reveal which of these proteins directly interact with HRASV12, or how these proteins interact with each other. This information is necessary for reconstructing HRAS induced protein interactome. Therefore, we used existing protein interaction databases, such as STRING, HPRD and SAPIN, and identified all interactions involving HRASV12, and the groups of proteins which appeared with higher intensities in our subcellular location specific dataset. We started with an empty network for each subcellular location, and populated each network with the corresponding HRASV12 formed interactome, reconstructed as described above. This step results in a PPI network that distinguishes between direct and indirect as well as known and new PPIs.

Step 2

The localization specific kinase-substrate interactions identified by analyzing the MS-phosphoproteomic screens were then added to the corresponding HRASV12 induced interactome. It is likely that some of the proteins identified in the interaction proteomic screens interact with some of the kinases involved in the kinase-substrate (K-S) interactions which were inferred from the phosphoproteomic data. However, neither the CoIP MS screens nor the phosphoproteomic MS screens allow us to identify such cross-omic interactions. Additionally, the activities of kinases were not directly measured in the phosphoproteomic screens but predicted from the phosphorylation levels of their substrates. Many of these kinases are known to interact with each other, but since they do not appear in the phosphoproteomic screens, it is not feasible to infer interactions between them from this data. Both of the above types of interactions are necessary to reconstruct HRAS induced multi-layer interactome. Therefore, we added all interactions (a) among the kinases of the localization specific phosphorylation networks form the STRING, HPRD, SAPIN, PhosphoELM and PhosphositePlus databases and (b) between HRASV12 interactomes and the kinases driving the activated HRAS induced phosphoproteome from the STRING, HPRD, SAPIN databases. For kinase-kinase interactions, we included interactions from both protein interaction (STRING, HPRD, SAPIN) and phosphorylation databases (PhosphoELM and PhosphositePlus) to reflect the fact that kinases can interact with each other by means of both protein binding and phosphorylation.

Step 3

Finally, we added the localization specific TRNs to each of the above networks. Again, neither the proteomic or transcriptomic datasets contain information to infer interactions between the HRAS induced interactome, phosphoproteome and the TFs regulating the TRNs. However, these interactions link the proteomic and transcriptomic layers of the network and are necessary to create the multilayer interaction network. Therefore, we added known PPIs (a) among RAS interactors and the TFs of the corresponding TRNs found in STRING, HPRD, SAPIN databases; and (b) between kinases, phosphoproteins and TFs of the corresponding TRNs found in the STRING, HPRD, SAPIN, PhosphoELM and PhosphositePlus databases. Interactions from both protein interaction and phosphorylation databases were used to reflect that fact that kinases can both bind to and phosphorylate TFs.

Each type of interaction described above was labeled using unique attributes such as PPI (protein-protein interaction), K-S (kinase-substrate interaction), GRN (gene regulatory network) as described in Table S4. Interactions which were not directly inferred from interaction/phospho-proteomics and transcriptomics data were labeled PREDICTED. Such labeling scheme allowed us to induce a spatial hierarchy in the combined network, e.g., interactions labeled with PPI, K-S and PREDICTED are protein layer interactions, whereas those labeled with GRN are transcription layer interactions.

QUANTIFICATION AND STATISTICAL ANALYSIS

The statistical analysis of the proteomics, phosphor-proteomics and transcriptomics data is explained in detail in their respective section. For the data in Figures 6 and 7, the bar graphs represent the mean and the error bars correspond to the standard errors of the mean (SEM). The difference between means of two groups was assessed using the t test. The value of n for the t test is the number of replicates and it is stated in the figure legends. The correlation with two variables was analyzed using Pearson's correlation coefficient. The statistical significance of Pearson's correlation coefficient (i.e., that the coefficient is different from zero) was tested using a t test with n-2 degrees of freedom, where n is the number of observations. P values under 0.05 were deemed significant.

DATA AND SOFTWARE AVAILABILITY

The mass spectrometry interaction proteomics and phosphoproteomics data reported in this paper have been deposited to the ProteomeXchange Consortium via the PRIDE (Perez-Riverol et al., 2019) partner repository with the accession numbers *ProteomeXchange:* PXD012505 and *ProteomeXchange:* PXD012506, respectively. The accession number for the DNA microarray data reported in this paper is ArrayExpress: E-MTAB-7672.

MATLAB and Java codes for the analysis of the interaction proteomics, phosphoproteomic, gene array data, network integration, and benchmarking of the kinase-substrate prediction are available in the supplementary folder "Codes for omics analysis & network integration."